Dynamics of Vorticity Defects in Stratified Shear

Anubhab Roy

October 19, 2010

1 Introduction

Stability of shear flows at high Reynolds number has been one of the cornerstones of hydrodynamic stability. A canonical problem which contains the basic features is that of a shear layer - two streams of different velocity flowing past each other with different density. Helmholtz[18] and Kelvin[21] were probably the earliest to consider evolution of disturbances in a stratified vortex sheet. While attempting a more general case Rayleigh[27] approximated the shear layer by piecewise-linear velocity profiles.

A kinematic description of the instability for the unstratified vortex sheet was given by Batchelor[1] purely based on vortex dynamics (figure 1(a)). Imagine perturbing the vortex sheet by a sinusoidal disturbance so that the perturbed interface is located at $\eta = \sin kx$. In the neighbourhood of the nodes (A and B), the positive vorticity induces a clockwise circulating velocity field. If $\partial\eta/\partial x > 0$, the crest and trough move away from each other, leading to vorticity being swept off from nodes like A, whereas if $\partial\eta/\partial x < 0$, the crest and trough come closer to each other, leading to vorticity being swept into nodes like B. Thus, accumulation of vorticity at points like B takes place unboundedly in the linear, non-dissipative scenario, giving exponential growth. In absence of stratification the vortex sheet problem as studied by Helmholtz and Kelvin is unstable to infinitely large wavenumbers. This ill-conditioned nature of the system gets removed in Rayleigh's problem with the introduction of a length scale (figure 1(b)). Rayleigh's problem consists of two interfaces of vorticity discontinuity. The Kelvin-Helmholtz (KH) instability of a shear layer was the

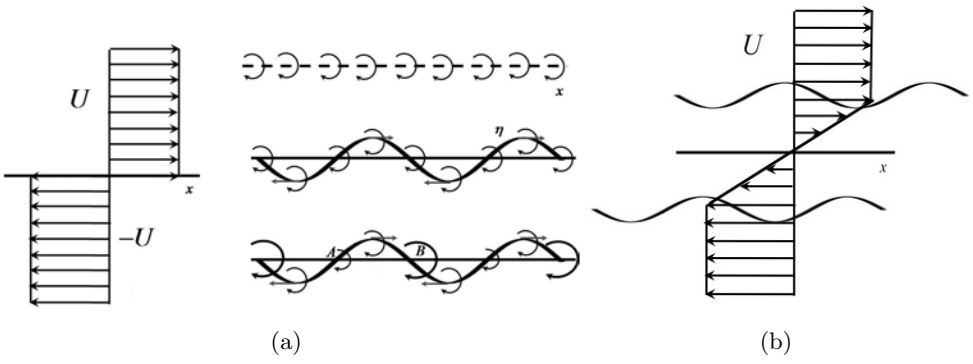

(a) (b)

Figure 1: (a) Vortex sheet (b) Mixing layer

Report Documentation Page

Form Approved
OMB No. 0704-0188

1. REPORT DATE	2. REPORT TYPE	3. DATES COVERED
19 OCT 2010		**00-00-2010 to 00-00-2010**

4. TITLE AND SUBTITLE	5a. CONTRACT NUMBER
Dynamics Of Vorticity Defects In Stratified Shear	5b. GRANT NUMBER
	5c. PROGRAM ELEMENT NUMBER
6. AUTHOR(S)	5d. PROJECT NUMBER
	5e. TASK NUMBER
	5f. WORK UNIT NUMBER
7. PERFORMING ORGANIZATION NAME(S) AND ADDRESS(ES) **Woods Hole Oceanographic Institution,Woods Hole,MA,02543**	8. PERFORMING ORGANIZATION REPORT NUMBER
9. SPONSORING/MONITORING AGENCY NAME(S) AND ADDRESS(ES)	10. SPONSOR/MONITOR'S ACRONYM(S)
	11. SPONSOR/MONITOR'S REPORT NUMBER(S)

12. DISTRIBUTION/AVAILABILITY STATEMENT
Approved for public release; distribution unlimited

13. SUPPLEMENTARY NOTES
See also ADA544302

14. ABSTRACT

15. SUBJECT TERMS

16. SECURITY CLASSIFICATION OF:			17. LIMITATION OF ABSTRACT	18. NUMBER OF PAGES	19a. NAME OF RESPONSIBLE PERSON
a. REPORT	b. ABSTRACT	c. THIS PAGE			
unclassified	**unclassified**	**unclassified**	**Same as Report (SAR)**	**33**	

(a) Mixing Layer - Lasheras and Choi (1988)

(b) The Meeting of Waters - Confluence of Rio Negro and Rio Solimões near Manaus, Brazil to form the Amazon (*Amazon Abyss*, BBC)

Figure 2: Kelvin-Helmholtz instabilties

earliest demonstrations of how inviscid instabilities can occur due to presence of vorticity extremum in the flow.
KH instability is commonly observed in nature. In atmospheric context clouds often help to visualise them. In figure 2 KH instabilities are seen in a laboratory experiment and also in rivers.

Though KH instability considers the two layers to be of two different density, for stable stratification the role of gravity is purely stabilising. Taylor[32] and Goldstein[17] simultaneously showed how stable stratification can have a destabilising role when it interacts with shear. Considering various multi-layer velocity/density profiles Taylor studied instabilities arising out of interaction of vorticity and/or gravity waves. We will revisit one of Taylor's problems later in the analysis.
Subsequently to model a stratified shear layer relevant for geophysical problems, Holmboe[20] considered Rayleigh's piecwise-linear approximation with an embedded density interface at the shear layer centre (figure 3). For weak stratification a KH like behaviour was observed, instabilities stationary with respect to the flow. On increasing stratification a new class of instabilities emerged - a pair of counter propagating waves known thereafter as Holmboe waves. Unlike KH instability Holmboe waves are not easily visualised in nature due to the nonstationary behaviour of the waves. They have been experimentally realised and considered to be present in exchange flows. Often a distinction is made between KH and Holmboe

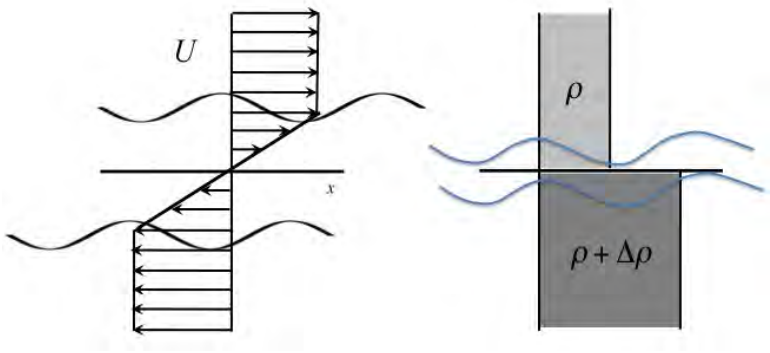

Figure 3: Stratified shear layer

waves based on the stationarity nature as one moves with the speed of the shear layer centre. Such a classification though accurate in the symmetrical case becomes ambiguous in the asymmetrical case. Recently[8] it was shown that a classification based on wave interactions - vorticity-vorticity or vorticity-gravity - provides a consistent explanation.
Approaches towards understanding evolution of disturbances in stratified shear layers can be mostly classified in two categories - Linear stability calculations and direct numerical simulations (DNS). While doing linear stability studies if one restricts to piecewise linear profiles then dispersion relations, eigenfunctions can be analytically computed. To model realistic profiles if one considers the smoother counterparts then solving the formidable Taylor-Goldstein equation (TGE) is the only recourse. For a complete nonlinear description beyond linear instability, DNS holds the key. DNS enables a complete exploration of wide range of length and time scales in flows transitioning towards a turbulent state. Having said that the computational cost and effort involved in a complete DNS severely limits an exhaustive study in nonlinear dynamics of stratified shear layers, many questions go unanswered. How does increasing stratification alter the nonlinear states in stratified shear layers? Does the flow attain a nonlinear stationary state? Gravity waves interact in presence of shear to give rise to Taylor-Caulfield instability, how does the nonlinear state evolve? To answer many such questions full nonlinear simulations are needed. Is there a reduced description of the governing equations which captures the essence of full numerical simulations while giving a stronger analytical handle on the physics? The goal of the present work is to outline a reductive perturbation theory for stratified shear layers. The methodology will rely on a previously used technique, the 'vorticity defect' method.

2 'Defect' theory

Inviscid shear flow instabilities occur in presence of vorticity maximum, e.g. - KH. For KH like flows one can immediately notice that the base-flow quantities vary across a very small region. This is also true for stratified shear layers where besides vorticity, variations of density occur over a small region. To obtain a reduced description we will try to exploit the smallness of the shear-layer thickness. The perturbative technique to be adopted will in spirit be akin to boundary layer theory. We will have an 'outer' region where the pertur-

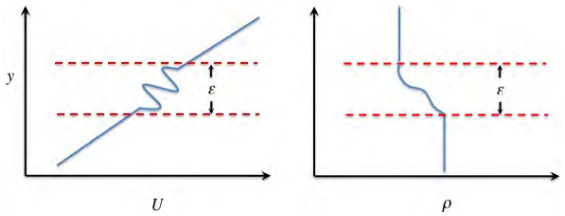

Figure 4: Velocity and density profiles with 'defects'

bations will be assumed to obey linear, steady and inviscid dynamics and an 'inner' region where nonlinearity, dissipation and unsteadiness will be important. A key assumption of the analysis will be considering the base-flow quantities (velocity, density) to be monotonically varying quantity with sharp variations or 'defects' of width ϵ at the shear layer centre.

While studying wake behind a airfoil, Gill[16] modelled the base-state to be a Couette flow with slight distortions. This severely simplified the linear stability calculations and provided integral dispersion relationships. Next Lerner and Knobloch[24] performed long-wavelength stability studies on a distorted Couette flow. The slight modification to Couette flow was assumed to arise due to finite amplitude perturbations. But it wasn't until the works of Balmforth and co-workers that the 'defect' model - a Couette flow with slight distortions - got a strong theoretical foundations and its immense applications appreciated. Using an analysis similar to critical layer theory del-Castillo Negrete et al.[15] (Balmforth et al. [3]) showed that for inviscid shear flows one can reduce 2D Euler equations to a nonlinear integro-differential equation for the 'defect' vorticity. Exploiting the 'defect' equations analogy with the Valsov-Poisson equation[1] explicit dispersion relations were obtained for various distortion imposed on the Couette flow. Balmforth and Young[5] went ahead and highlighted evaluation of nonlinear stationary states from the 'defect' equations. The linear viscous problem was addressed by Balmforth [6] and the intriguing connection between viscous and inviscid eigensolutions was discussed in context to various 'defect' profiles. The applicability of the approach for visco-elastic flows has also been studied[4]. In the present work we will try to obtain better understanding of stratified shear layers aided by the 'defect' theory.

Consider a Bousinessq fluid of density,

$$\rho(x, y, t) = \rho_m + \delta\rho(x, y, t) \tag{1}$$

The evolution equations, vorticity-buoyancy formulation, in the Bousinessq approximation can be written in the following non-dimensional form,

$$\frac{\partial \omega}{\partial t} + \frac{\partial(\Psi, \omega)}{\partial(x, y)} = \frac{\partial B}{\partial x} + \frac{1}{Re}\nabla^2\omega \tag{2}$$

$$\frac{\partial B}{\partial t} + \frac{\partial(\Psi, B)}{\partial(x, y)} = \frac{1}{ReSc}\nabla^2 B \tag{3}$$

[1]Vlasov-Poisson equation describes time evolution of the distribution function of plasma consisting of collision-less charged particles in the zero magnetic field limit.

The horizontal and vertical coordinates have been non-dimensionalised by a characteristic length-scale L_0 and time by U_0/L_0, U_0 being a velocity scale. Stream-function is non-dimensionalised by $U_0 L_0$. $\omega = \nabla^2\Psi$ and $B = -g\delta\rho/\rho_m L_0/U_0^2$ are the non-dimensional vorticity and buoyancy respectively. Reynolds number, $Re = U_0 L_0/\nu$ (ν is the kinematic viscosity), denotes a ratio of inertial to viscous forces and Schmidt number, $Sc = \nu/\kappa$ (κ is the mass diffusivity), provides a ratio of momentum to mass diffusivity. We will focus on $Sc \to \infty$, the relevant regime for stratified shear layers[2].
As evident in figure 4, velocity is assumed to be a localised 'defect' imposed on a Couette flow and similarly buoyancy remains largely uniform but for a sharp variation at the 'defect' level. Thus if the variations occur over a length-scale ϵ, we can write,

$$\Psi = -\frac{1}{2}y^2 + \epsilon^2\psi(x, y, t) \tag{4}$$

$$B = b_m + \epsilon^2 b \tag{5}$$

Hence the vorticity-buoyancy equation can be reduced to,

$$\nabla^2\psi_t + y\nabla^2\psi_x + \epsilon^2(\psi_x\nabla^2\psi_y - \psi_y\nabla^2\psi_x) = b_x + Re^{-1}\nabla^4\psi \tag{6}$$

$$b_t + yb_x + \epsilon^2(\psi_x b_y - \psi_y b_x) = (ReSc)^{-1}\nabla^2 b \tag{7}$$

The above equations can be solved using matched asymptotic theory by splitting the flow into an exterior region where base flow quantities remain uniform or vary monotonically and an interior region corresponding to the 'defect'.

2.1 Outer solution

The dynamics in the outer region is assumed to be steady, inviscid and linear in the leading order. Another important assumption made regarding the outer solution is that of weak stratification. It is assumed that the outer solution for ψ, in the leading order, is uninfluenced by buoyancy. As would become evident that in doing so we deal with a weaker singularity in the outer problem. An assumption of these form becomes unphysical for strongly stratified flows, scenarios beyond the scope of stratified 'defects'.
A regular perturbation expansion of the solution in the outer region provides,

$$\psi = \psi_0 + \epsilon\psi_1 + \dots \tag{8}$$

$$b = \epsilon b_1 + \dots \tag{9}$$

Thus the leading order dynamics is governed by the following pair of equations.

$$y\nabla^2\psi_{0x} = 0, \quad yb_{1x} = 0 \tag{10}$$

$$\Rightarrow \quad \nabla^2\psi_0 = -2A(x,t)\delta(y) \tag{11}$$

Thus the outer solution behaves like an irrotational flow being forced by a vortex sheet, a δ function singularity, at the 'defect' level - $y = 0$ (buoyancy also gets forced by a density

[2]In the context of passive scalar turbulence $Sc \to \infty$ is known as the Batchelor regime. Such a regime allows for rapid variations in passive scalar field due to stirring by a smooth velocity field.

sheet). This necessitates a jump in tangential velocity (while maintaining continuity of normal velocity),

$$[\psi_{0y}]_{y=0^-}^{y=0^+} = -2A(x,t), \qquad [\psi_0]_{y=0^-}^{y=0^+} = 0 \tag{12}$$

As will be seen this jump in the outer solution will be smoothened out over a region ϵ by the inner solution. If we had allowed for leading order buoyancy effects in the outer vorticity equation, the flow would have been forced by a vortex dipole instead of a vortex sheet. The consequence of these stronger singularity, a δ' singularity, would have then resulted in a jump in normal velocity. Weak stratification allows us to overlook such a possibility in the present analysis.
Introducing Fourier transform of the streamfunction as,

$$\tilde{\psi}(k,y,t) = \mathcal{F}[\psi(x,y,t)] = \int_{-\infty}^{\infty} \psi(x,y,t)e^{-ikx}dx \tag{13}$$

equation 11 can be written as,

$$\tilde{\psi}_{0yy} - k^2\tilde{\psi}_0 = -2\tilde{A}(k,t)\delta(y) \tag{14}$$

Thus one obtains,

$$\psi_0 = \mathcal{F}^{-1}\left[\mathcal{G}(k)\hat{A}(k,t)\right] \tag{15}$$

where, $\mathcal{F}^{-1}$ denotes the inverse Fourier transform and the Green's function, $\mathcal{G}(k)$, can be computed for both unbounded and bounded domains ($|y| \leqslant 1$) as,

$$\mathcal{G}(k) = \frac{1}{|k|}\text{sech}|k|\sinh|k|(1-|y|), \qquad \text{bounded} \tag{16}$$

$$= \frac{1}{|k|}e^{-|k||y|}, \qquad \text{unbounded} \tag{17}$$

Henceforth all analysis will be presented for the unbounded case but the results have been extended to the bounded case too. The 'defect' analysis is not solely restricted to the outer flow being Couette and can be extended to more general flows by the method of constructing Green's function for flow profiles with curvature[2].
Next we will regularise the discontinuity in outer velocity field by evaluating the inner solution.

2.2 Inner solution

Similar to a traditional boundary-layer like analysis, the inner solution must contain at least one of the physics that have been overlooked in the outer region - viscosity, nonlinearity and unsteadiness. Working with our small parameter, the defect thickness ϵ, we define a stretched vertical coordinate, $\eta = y/\epsilon$ and a slow time-scale $\tau = \epsilon t$. It needs to be mentioned that the method of analysis bears similarities with standard critical layer theories ([33],[31]). Beyond the initial transients the $O(\epsilon^2)$ nonlinear term acting on a critical layer of width $O(\epsilon)$ becomes important after time $O(1/\epsilon)$. As would become clear that the 'defect' theory

is considerably simpler than critical layer analysis. We pose the following expansion in the inner variables,

$$\psi = \psi_0(x,0,t) + \epsilon\phi_1(x,\eta,\tau) + O(\epsilon^2), \tag{18}$$

$$\Rightarrow \quad \psi_y = \phi_{1\eta} + \epsilon\phi_{2\eta} + O(\epsilon^2), \tag{19}$$

$$\Rightarrow \quad \nabla^2\psi = \epsilon^{-1}\phi_{1\eta\eta} + \psi_{0xx} + \phi_{2\eta\eta} + O(\epsilon) \tag{20}$$

$$b = \mathcal{B}(x,\eta,\tau) + O(\epsilon) \tag{21}$$

From above equations it is evident that leading order inner solution, $\psi_0(x,0,t)$, matches the corresponding outer solution at $y = 0$. As mentioned before the discontinuity in tangential velocity in the outer solution will be smoothed by the inner solution,

$$2A(x,t) = -\int_{-\infty}^{\infty} \mathcal{Z} d\eta \tag{22}$$

where $\mathcal{Z} = \phi_{1\eta\eta}$ is the leading order defect vorticity. The velocity jump equals the vorticity integrated across the defect.

Substituting the expansion 18 in equations 6 and 7 and collecting the leading order terms one obtains the 'defect' vorticity-buoyancy equations,

$$\mathcal{Z}_\tau + \eta\mathcal{Z}_x + \Phi_x\mathcal{Z}_\eta = \mathcal{B}_x + \lambda Z_{\eta\eta}, \tag{23}$$

$$\mathcal{B}_\tau + \eta\mathcal{B}_x + \Phi_x\mathcal{B}_\eta = \frac{\lambda}{Sc} B_{\eta\eta}, \tag{24}$$

$$(\mathcal{Z},\mathcal{B}) \to 0, \text{ as } |\eta| \to \infty$$

$$\tilde{\Phi} = -\frac{1}{2|k|}\int_{-\infty}^{\infty} \tilde{\mathcal{Z}} d\eta, \quad \Rightarrow \mathcal{H}(\Phi)_x = -\frac{1}{2\pi}\int_{-\infty}^{\infty} \mathcal{Z} d\eta \tag{25}$$

where, $\mathcal{H}(.)$ denotes the Hilbert transform of a variable defined in terms of the following Cauchy principal value integral,

$$\mathcal{H}(u) = \frac{1}{\pi} \fint \frac{u(\xi)}{\zeta - \xi} d\xi \tag{26}$$

and $\lambda = (\epsilon^3 Re)^{-1}$ is representative of the ratio of nonlinearity and viscosity. In critical layer theory there exists a similar quantity, Haberman parameter, which denotes competition of nonlinearity and viscosity.

Equations 23-25 are the 'defect' vorticity-buoyancy equations relevant for stratified shear layer studies. During the course of reduction we have retained the necessary physics due to unsteadiness, nonlinearity and dissipation. Though the obtained nonlinear integro-differential equations appear more daunting than the governing equations we started off with it would become clear that the 'defect' equations are more amenable to analytical and numerical treatments. Similar equations have been derived in critical layer theories for stratified shear flows [14].

3 Conservation laws

The inviscid, nonlinear 'defect' equations (equation 23-24 for $\lambda = 0$) contains certain conserved quantities, some deducible from evident symmetries in the problem and others not so obvious ones. Lets us define a spatial average,

$$< . >= \int \int .dxd\eta$$

In absence of dissipation both average vorticity and buoyancy remains conserved,

$$< \mathcal{Z} >_\tau = 0, \quad < \mathcal{B} >_\tau = 0 \tag{27}$$

momentum remains conserved,

$$< \eta\mathcal{Z} >_\tau = 0 \tag{28}$$

and energy also is conserved,

$$< \frac{\eta^2 - \Phi}{2}\mathcal{Z} - \eta\mathcal{B} >_\tau = 0 \tag{29}$$

As always is the case with ideal fluid besides the above ones there exists an infinitude of conserved quantities - Casimirs. For 2D homogeneous fluid any functional of vorticity is a conserved quantity. Enstrophy - a representative of vortex stretching and tilting - is one such commonly used candidate. For stratified flows due to baroclinic generation of vorticity enstrophy is no longer conserved. For stratified 'defects' one instead has the any functional of buoyancy and product of vorticity with any buoyancy functional as the Casimirs,

$$< G(\mathcal{B}) >_\tau = 0, < \mathcal{Z}F(\mathcal{B}) >_\tau = 0 \tag{30}$$

The conserved quantities thus obtained help in obtaining the stationary states for the system and also comment on its nonlinear stability. More importantly it also helps as a check in numerical computations to ensure that the numerical method indeed conserve the necessary invariants.

4 Inviscid linear stability

Earlier it was mentioned that previous studies on flow with slight distortions exploited the simplicity of the model in deriving explicit integral dispersion relations. Conventionally inviscid linear stability demands solution of Rayleigh equation or in the case of stratified shear flow Taylor Goldstein equation (TGE),

$$\left[\frac{d^2}{dy^2} - k^2\right]\hat{\psi} = \frac{\bar{U}''\hat{\psi}}{(\bar{U} - c)} - \frac{N^2\hat{\psi}}{(\bar{U} - c)^2} \tag{31}$$

where $\hat{\psi}$ is the disturbance streamfunction, $\bar{U}$ the background base-flow, $N = \sqrt{-g/\rho_m d\rho/dz}$ the BruntVäisälä (buoyancy time-scale), k is the disturbance wave-number and c is the wave-speed. The relative strength of stratification vis-a-vis inertia is denoted by Richardson

number, $Ri = (NL_0/U_0)^2$. Solution of the above boundary value problem, even numerically, is no easy task and analytical solutions can be obtained only for broken-line profiles. The 'defect' model circumvents this difficulty with ease.
Consider the 'defect' vorticity and buoyancy to be decomposed of a base-state contribution and a perturbation,

$$\mathcal{Z}(x,\eta,\tau) = F(\eta) + \zeta(x,\eta,\tau) \tag{32}$$

$$\mathcal{B}(x,\eta,\tau) = \int^{\eta} N^2(y)dy + \beta(x,\eta,\tau) \tag{33}$$

Substituting the above expressions in equations 23 and 24 and considering the linearised equations one has,

$$\zeta_\tau + \eta\zeta_x + r_x F_\eta = \beta_x, \tag{34}$$

$$\beta_\tau + \eta\beta_x + r_x N^2 = 0 \tag{35}$$

$$2\hat{r} = -k^{-1}\int_{-\infty}^{\infty} \hat{\zeta} d\eta \tag{36}$$

On assuming a normal-mode form, $\zeta(x,\eta,\tau) = \hat{\zeta}(\eta)e^{ik(x-c\tau)}$, the eigenfunctions can be expressed as,

$$\hat{\beta} = -\frac{\hat{r}N^2}{(\eta - c)}, \tag{37}$$

$$\hat{\zeta} = -\frac{\hat{r}F_\eta}{(\eta - c)} - \frac{\hat{r}N^2}{(\eta - c)^2} \tag{38}$$

and the dispersion relation,

$$\mathcal{D}(c,k;F,N) \equiv 2k - \int_{-\infty}^{\infty}\left[\frac{F_\eta}{(\eta - c)} + \frac{N^2}{(\eta - c)^2}\right] d\eta = 0 \tag{39}$$

This is the stratified version of the integral dispersion relation obtained in [3]. $\mathcal{D}$ is an analytic function of c but for the real-axis where it has a branch-cut. The branch-cut gives rise to the continuous spectrum, a common feature of inviscid shear flows. The presence of the continuous spectrum contributes to transient growth in flows which otherwise are modally stable - Orr mechanism being a well known example. Sometimes the dispersion relation instead of having zeros in the principal complex plane, vanishes at points on different Riemann sheets. While doing the initial value problem this leads to observation of a collective behaviour of the continuous spectrum as a single damped discrete mode - known as Landau pole or quasi-mode. This damping, eponymously known as Landau damping in plasma physics, is a purely inviscid phenomenon arising due to phase mixing. Quasi-modes have been probed to understand the mysterious connection between the inviscid and viscous initial value problem in the limit of vanishing viscosity. The present analysis will focus purely on unstable modes and hence no longer address the above intriguing phenomena.
We will now compute dispersion relations for various stratified shear layer configurations. Before proceeding on to calculations for both broken and smooth profiles a note can be

made borrowing from Nyquist theory. For a closed curve $\mathcal{C}$ in the complex c plane, the winding number,

$$\frac{1}{2\pi i}\oint_{\mathcal{C}}\frac{\mathcal{D}'(c)}{\mathcal{D}(c)}dc = \text{N-P} \tag{40}$$

where N is the number of zeros and P gives the number of poles of $\mathcal{D}(c)$ inside $\mathcal{C}$. Considering $\mathcal{D}$ an analytic function of c the winding number gives us the number of eigenmodes. Earlier works on 'defect' theory like [3] and [6] elucidates how Nyquist theory can be used effectively for the 'defect' model.

4.1 Holmboe instability

Holmboe instability occurs when there exists a density interface embedded in a mixing layer. It is a popular model to represent instabilities arising due to horizontal shearing of density interfaces. This classical instability, in the symmetrical case, exhibits a transition from the stationary Kelvin-Helmholtz instability to the propagating Holmboe waves. Though Holmboe waves are inherently difficult to visualise in nature due to their non-stationary behaviour they have been observed in laboratory experiments - exchange flow between two basins of different density being an example.

4.1.1 Broken-line profile

For a broken-line Holmboe profile denoted by the following defect vorticity and buoyancy profile,

$$F_\eta = f[\delta(\eta-\eta_0)-\delta(\eta+\eta_0)], \tag{41}$$

$$N^2 = d\delta(\eta) \tag{42}$$

one obtains the dispersion relation,

$$c^4 - \left(1-\frac{f}{k}+\frac{d}{2k}\right)c^2 + \frac{d}{2k} = 0, \qquad \eta_0 = 1, c = c_r + ic_i \tag{43}$$

It was previously mentioned that the 'defect' theory is suited to weak stratification calculations. Thus the results obtained are representative of small Ri cases in the complete problem. d determines the strength of stratification and a qualitative comparison is made of contours of growth-rate in $d-k$ plane with the one obtained from the solution of TGE for a symmetric shear layer. The basic features are well captured by the present model (figure 5). One immediate observation is the differentiation of stationary ($c_r = 0$) and propagating instabilities ($c_r \neq 0$).

4.1.2 Smooth profile

For smooth profiles the integral dispersion relation can be evaluated using Cauchy residue theorem. The simplest profile to consider would be a Lorentzian.

$$F_\eta = \frac{\alpha f}{\pi}\left[\frac{1}{(\eta+1)^2+\alpha^2} - \frac{1}{(\eta-1)^2+\alpha^2}\right], \tag{44}$$

$$N^2 = \frac{\alpha d}{\pi}\frac{1}{\eta^2+\alpha^2} \tag{45}$$

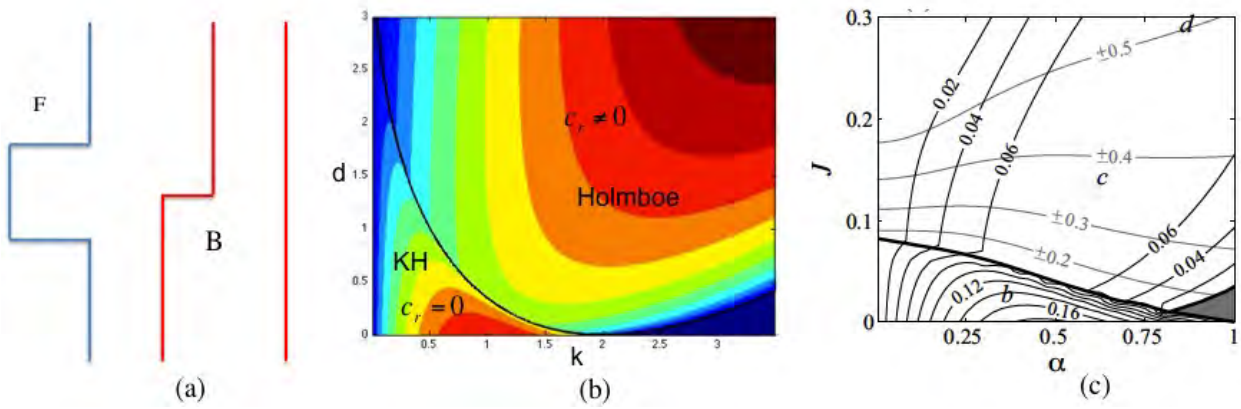

Figure 5: Holmboe instability. a) A broken-line profile, b) Contours of growth-rate (c_i) in $d-k$ plane ($f=2$), c) Growth-rate contours in $Ri-k$ plane from a complete linear stability calculations (Carpenter et al.[8])

For the Lorentzian profile the dispersion relation is identical to equation 43 with c in the quadratic expression no longer being the complex wave-speed but instead replaced by $c \to c + i\alpha\,\mathrm{sgn}(c_i)$.
A smooth profile which would be used in the numerical calculations and represents sharper variations in flow quantities is a tanh profile.

$$F = \frac{f}{2}\left[\tanh\left(\frac{\eta-\eta_0}{\Delta}\right) - \tanh\left(\frac{\eta+\eta_0}{\Delta}\right)\right] \tag{46}$$

$$N^2 = \frac{d}{2\Delta}\mathrm{sech}^2\left(\frac{\eta}{\Delta}\right) \tag{47}$$

One could note that the both the smooth profiles chosen above are functions which are nascent delta functions, i.e. as $\alpha, \Delta \to 0$ we obtain the generalised functions form as given in equation 42.
From residue calculus we can evaluate the following integrals,

$$\mathcal{I}_1(\Delta,\eta_0,c) = \int_{-\infty}^{\infty} \frac{\mathrm{sech}^2\left(\frac{\eta-\eta_0}{\Delta}\right)}{(\eta-c)} d\eta = 2\pi i\left[\mathrm{sech}^2\left(\frac{c-\eta_0}{\Delta}\right)s - \frac{1}{\pi^2}\Psi^{(1)}(\alpha)\right]$$

$$\mathcal{I}_2(\Delta,\eta_0,c) = \int_{-\infty}^{\infty} \frac{\mathrm{sech}^2\left(\frac{\eta-\eta_0}{\Delta}\right)}{(\eta-c)^2} d\eta = -\frac{2\pi i}{\Delta}\left[2\mathrm{sech}^2\left(\frac{c-\eta_0}{\Delta}\right)\tanh\left(\frac{c-\eta_0}{\Delta}\right)s + \frac{i}{\pi^3}\Psi^{(2)}(\alpha)\right]$$

$$\alpha = \frac{1}{2} - \frac{i}{\pi\Delta}(\eta_0 - c), \qquad s = \frac{1}{2}(1+\mathrm{sgn}(c_i))$$

where $\Psi^{(1)}(\alpha)$ and $\Psi^{(2)}(\alpha)$ are polygamma functions - $\Psi^{(n)}(z) = d^{n+1}(\log\Gamma(z))/dz^{n+1}$. Based on the above evaluated integrals the dispersion relation for the tanh Holmboe profile can be computed explicitly as,

$$2k - \frac{1}{2\Delta}\left[f\left\{\mathcal{I}_1(\Delta,\eta_0,c) - \mathcal{I}_1(\Delta,-\eta_0,c)\right\} + d\,\mathcal{I}_2(\Delta,0,c)\right] = 0 \tag{48}$$

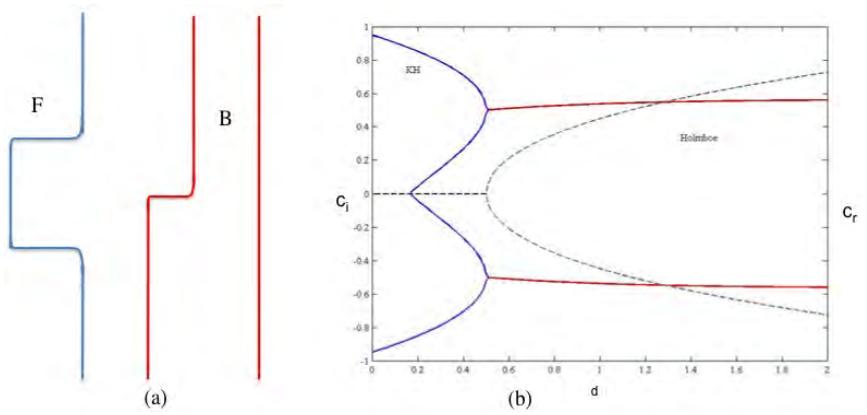

Figure 6: Holmboe instability. a) A Smooth profile, b) Variation of c_r (dashed) and c_i (continuous) with stratification (d) for $f = 2, k = 1, \Delta = 1/3, \eta_0 = 1$

Though we have obtained an analytical dispersion relation for the tanh profile the numerical evaluation of the integrals is more efficient than working with the polygamma functions.

Figure 6 shows the stationary and propagating nature of the instabilities for a set of parameter values. Cases from the instability curves will be later visited during numerics. An important question that numerics will try to answer is how does the nonlinear states change as one increases stratification and transitions from a KH instability to Holmboe instability.

4.2 Taylor-Caulfield instability

Holmboe instability arose when gravity waves interacted with vorticity waves. Taylor[32] during the course of studying various broken line profiles observed that a stable stratification composed of two density jumps gets destabilised if there is an imposed shear. This initially surprising result can be understood as interaction of gravity waves facilitated by shear.

4.2.1 Broken-line profile

For Taylor-Caulfield instabilities there is no defect vorticity and instead one has variations of defect buoyancy,

$$N^2 = d[\delta(\eta - \eta_0) + \delta(\eta + \eta_0)]) \tag{49}$$

As seen in the case of Holmboe instability one obtains polynomial dispersion relations for broken-line profiles,

$$c^4 - \left(2 + \frac{d}{k}\right) c^2 + \left(1 - \frac{d}{k}\right) = 0, \qquad \eta_0 = 1, c = c_r + ic_i \tag{50}$$

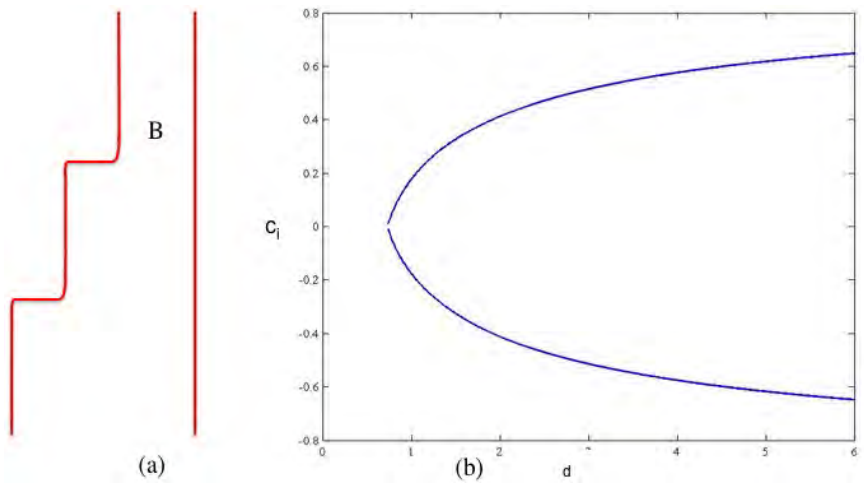

Figure 7: Taylor-Caulfield instability. (a) A Smooth profile, (b) Growth-rate (c_i) variation with stratification (d) for $k = 1, \eta_0 = 1$

4.2.2 Smooth profile

Similar to Holmboe case one can calculate stability characteristics for various smooth profiles. For a Lorentzian profile,

$$N^2 = \frac{\alpha d}{\pi}\left[\frac{1}{(\eta+1)^2+\alpha^2} + \frac{1}{(\eta-1)^2+\alpha^2}\right] \tag{51}$$

The dispersion relation is identical to equation 50 with c in the quadratic expression no longer being the complex wave-speed but instead replaced by $c \to c + i\alpha\,\mathrm{sgn}(c_i)$.
For a smooth tanh profile,

$$N^2 = \frac{d}{2\Delta}\left[\mathrm{sech}^2\left(\frac{\eta-\eta_0}{\Delta}\right) + \mathrm{sech}^2\left(\frac{\eta+\eta_0}{\Delta}\right)\right] \tag{52}$$

Once again the analytical form of the dispersion relation for can be written as,

$$2k - \frac{d}{2\Delta}[\mathcal{I}_2(\Delta,\eta_0,c) + \mathcal{I}_2(\Delta,-\eta_0,c)] = 0 \tag{53}$$

Figure 7 illustrates the stability characteristics for Taylor-Caulfield instability as obtained from 'defect' theory. The TC modes are purely stationary waves.

Though there exists some linear stability calculations and DNS calculations very little is known about the nonlinear states of Taylor-Caulfield instabilities. Next using numerical solution of 'defect' equations we will try to explore the details.

5 Numerical solution

A significant advantage that the 'defect' theory offers over the complete Bousinnessq Navier-Stokes equations is in numerical computation. As is commonly known that the notorious

advective nonlinearity in Navier-Stokes serves as a severe bottleneck in full-fledged computations. The defect equations for $Sc \to \infty$,

$$\mathcal{Z}_\tau + \eta \mathcal{Z}_x + \Phi_x \mathcal{Z}_\eta = \mathcal{B}_x + \lambda Z_{\eta\eta}, \tag{54}$$

$$\mathcal{B}_\tau + \eta \mathcal{B}_x + \Phi_x \mathcal{B}_\eta = 0, \tag{55}$$

$$(\mathcal{Z}, \mathcal{B}) \to 0, \text{ as } |\eta| \to \infty$$

$$\tilde{\Phi} = -\frac{1}{2|k|} \int_{-\infty}^{\infty} \tilde{\mathcal{Z}} d\eta, \quad \Rightarrow \mathcal{H}(\Phi)_x = -\frac{1}{2} \int_{-\infty}^{\infty} \mathcal{Z} d\eta \tag{56}$$

though nonlinear avoids the difficult nonlinearity $\partial(\phi_1, \phi_{1\eta\eta})/\partial(x, \eta)$ ($\phi_{1\eta\eta} = \mathcal{Z}$). In the present form the 'defect' equation entails solving a set of advection-diffusion equations. The method adopted in the present work relies on exploiting the similarities of the 'defect' equations with the Vlasov-Poisson equation and using a operator-splitting technique.

5.1 Operator splitting technique

The operator splitting technique used is based on the method outlined in [13] for solution of Vlasov-Poisson equation and in [7] for studying critical layers in 2D vortices. This splitting technique is also known as Strang splitting[25].
The integration over time-step $[\tau, \tau + \delta\tau]$ is divided into three stages,

5.1.1 Advect in x for half time-step

Consider the advection in x in the buoyancy equation,

$$\mathcal{B}_\tau + \eta \mathcal{B}_x = 0 \tag{57}$$

for a time interval $\delta\tau/2$. The exact solution is $\mathcal{B}(x, \eta, \tau + \delta\tau/2) = \mathcal{B}(x - \eta\delta\tau/2, \eta, \tau)$. Fourier interpolation is used to perform the x advection - $\tilde{\mathcal{B}}(k, \eta, \tau + \delta\tau/2) = \tilde{\mathcal{B}}(k, \eta, \tau) e^{-ik\eta\delta\tau/2}$. For the vorticity equation,

$$\mathcal{Z}_\tau + \eta \mathcal{Z}_x = \mathcal{B}_x \tag{58}$$

the solution can be similarly written in Fourier space as -

$$\tilde{\mathcal{Z}}(k, \eta, \tau + \delta\tau/2) = \tilde{\mathcal{Z}}(k, \eta, \tau) e^{-ik\eta\delta\tau/2} + ik\delta\tau/2\, \tilde{\mathcal{B}}(k, \eta, \tau + \delta\tau/2)$$

The above calculations in Fourier space is done using the FFT/IFFT routine in Matlab.

5.1.2 Advect in η for a complete time-step

Both buoyancy and vorticity obeys identical η advection equation,

$$\mathcal{B}_\tau + \Phi_x \mathcal{B}_\eta = 0 \tag{59}$$

$$\tilde{\Phi} = -\frac{1}{2|k|} \int_{-\infty}^{\infty} \tilde{\mathcal{Z}} d\eta \tag{60}$$

Before performing the advection Φ_x is computed by integrating $\mathcal{Z}$ in η, once again in Fourier space. The η advection occurs with a velocity Φ_x - $\mathcal{B}(x, \eta, \tau + \delta\tau) = \mathcal{B}(x, \eta - \Phi_x \delta\tau, \tau)$. Due

to lack of periodicity we use linear/cubic spline interpolation in η instead of Fourier. The same method is followed for advection of $\mathcal{Z}$. If advection happens into the domain from both above or below the computational domain then it is assigned the far-field equilibrium value.

5.1.3 Advect in x for another half time-step

The first step is repeated for another half time-step, $\delta\tau/2$. One can combine the first and third step and do two steps instead - advect in η for $\delta\tau$ followed by advection in x for another $\delta\tau$.

To account for diffusion of vorticity ($\lambda \neq 0$) a forward in time Euler integration is carried out with diffusion operator in η discretized using finite-difference technique.

The computational domain consists of $(x, \eta) \in [0, 2\pi] \times [-\eta_{max}, \eta_{max}]$. η_{max} is fixed at 10 so that the vertical extent is at least 5 times larger than the shear layer and the far-field is ensured to remain uninfluenced by the dynamics in the shear layer. The choice of time-step, $\delta\tau$, and horizontal discretization, $h = 2\pi/N$, (N is the number of Fourier modes used) is determined by the following stability condition,

$$|\eta_{max}|\Delta\tau \leqslant h \tag{61}$$

For the present work N has been chosen to either 256 or 512 and the time-step, $\Delta\tau = 1\times10^{-4}, 5\times10^{-4}$. The vertical discretization, $\Delta\eta$, is chosen so as to obey the von Neumann stability criteria,

$$\frac{\lambda\Delta\tau}{(\Delta\eta)^2} \leqslant \frac{1}{2} \tag{62}$$

$\Delta\eta = 0.01, 0.005$ is used in the calculations. λ, an estimate for momentum diffusion, has been widely varied from $0.05 - 10^{-4}$. All numerics reported hereafter are for $\lambda = 10^{-3}$. To instigate instabilities in the flows the base-state is initially seeded with a disturbance of the form $e^{-\eta^2}\cos kx$ of magnitude 0.1% of the base-state maxima. The η interpolation has been done using linear interpolation. The interp1 command in Matlab has been used for the purpose. For stratified KH (section 5.3.1) a grid resolution of 256×2001 has been used with a time-stepping of 5×10^{-4}. The remaining calculations have been done on a 512×4001 grid with $\Delta\tau = 1 \times 10^{-4}$.

5.2 Analytical comparisons

To check the efficacy of the operator splitting technique a comparison is made between the numerical solution and analytical solution known for a passive scalar advection equation. The passive scalar advection equation,

$$\chi_\tau + \eta\chi_x + 2\chi_\eta \cos 2x = 0 \tag{63}$$

was studied by Stewartson[31] in the context of critical layers. The above equation can be solved using method of characteristics and drawing analogy with motion of pendulum. For

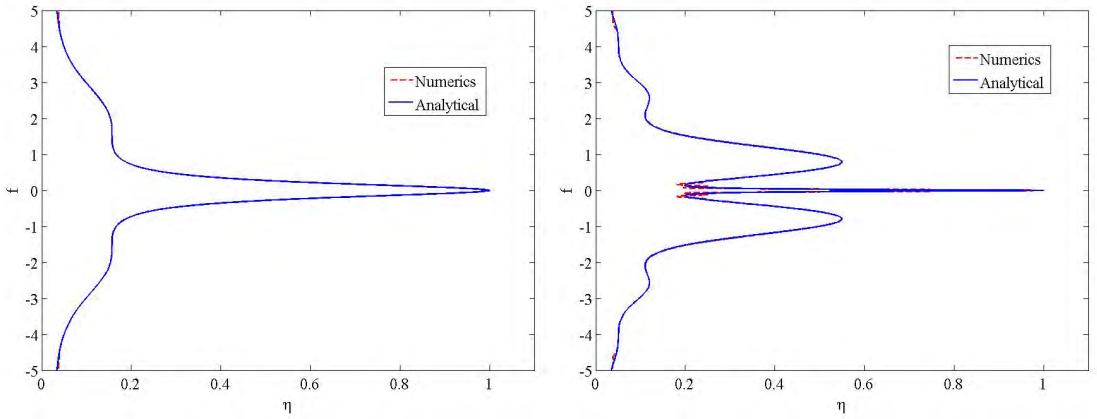

(a) $t = 1$ (b) $t = 2$

Figure 8: Comparison of analytical and numerical results for the passive scalar problem at $x = 3\pi/4$. χ is $\chi(3\pi/4, \eta, 0) = 1/(1+\eta^2)$

$x = \pi/4$ or $3\pi/4$ one can obtain explicit expressions for χ. At $x = 3\pi/4$ if initially the distribution of χ is $\chi(3\pi/4, \eta, 0) = f(\eta)$ then the solution at arbitrary times will be[7],

$$\chi\left(\frac{3\pi}{4}, \eta, \tau\right) = f\left(\frac{2\,\mathrm{sgn}(\eta)}{\sqrt{m}}\mathrm{dn}\left(\mathrm{K}(m) - \frac{2\tau}{\sqrt{m}}\right)\right),\ m = \frac{4}{4+\eta^2} \tag{64}$$

where dn is the Jacobi elliptic function and $\mathrm{K}(m)$ the complete elliptic integral of first kind. Figure 8 shows the good agreement between numerical and analytical results for a Lorentzian initial condition. The agreement starts deteriorating with time due to generation of increasing fine-scales.

5.3 Holmboe instabilities

By increasing stratification we will try to explore various nonlinear dynamics for instability scenarios occurring in Holmboe instabilities starting from stratified KH and proceeding on to pure Holmboe waves. For the purpose of exploring various nonlinear states the tanh model discussed before is revisited.

$$F = \frac{f}{2}\left[\tanh\left(\frac{\eta - \eta_0}{\Delta}\right) - \tanh\left(\frac{\eta + \eta_0}{\Delta}\right)\right] \tag{65}$$

$$N^2 = \frac{d}{2\Delta}\mathrm{sech}^2\left(\frac{\eta}{\Delta}\right) \tag{66}$$

$f = 2, k = 1, \Delta = 1/3, \eta_0 = 1$ are the parameters maintained identical for all Holmboe simulations. We choose 3 values of d. $d = 0.1, 1.5\,\&\,8$. As visible from figure 6, $d = 0.1$ denotes stationary stratified KH waves in linear regime, $d = 1.5, 8$ denote linear propagating Holmboe waves ($d = 8$ is not shown in the figure). We will try to find how the nonlinear states behave for these cases. Does a linear Holmboe wave remain so always howsoever weak the stratification may be?

5.3.1 Stratified KH ($d = 0.1$)

Kelvin-Helmholtz in presence of weak stratification contains all the usual traits of the unstratified version - growth of instability waves, roll-up of the shear layer, vortex nutation (the horizontal rocking of partially form cat's eye) and finally culminating with the celebrated cat's eye pattern or the KH billow. Besides the weakened growth-rate due to the stabilising effect of stratification the stratified version exhibits intense stirring and mixing of the buoyancy field. 3D effects like elliptical instability of the billow and hyperbolic instability of the braid also emerge later in the evolution. Interested reader can find detailed discussions in the article by Caulfield and Peltier[12].
Figure 9 shows the evolution of buoyancy ($\mathcal{B}$) and vorticity ($\mathcal{Z}$) field at different instants of time. Figure 9(a)-(b) is a snapshot when the flow exhibits finite amplitude waves just prior to the roll-up. (c)-(d) is at a stage during the formation of the billow. The flow has departed from linear stability predictions and vortex nutations are observed at this stage. Finally in figure 9(e)-(f) the well homogenised KH billow is visible. Figure 10 shows the time-evolution of $< |\psi|^2 >^{1/2}$, a measure of disturbance amplification. Signatures of the features discussed above can be seen in the time-trace.

5.3.2 Pure Holmboe ($d = 8$)

Next we explore a case where the flow is buoyancy dominant and the shear layer dynamics are very different from KH. For strongly stratified shear layers the flow exhibits propagating Holmboe instabilities. They are identified by oppositely travelling cusps which spews fluid from one region to other. Compared to a KH billow the Holmboe waves are highly inefficient in mixing. The dynamics is very often given by the beating phenomena of the two Holmboe waves. Laboratory experiments on Holmboe waves have been done by Lawrence et al. [22], Pouliquen et al.[26] and several researchers thereafter. Efforts towards using DNS to understand Holmboe wave dynamics was done by Smyth and co-workers ([28], [29] and [30]) amongst others. A recent work by Carpenter et al.[9] considers both experimental and numerical simulation aspects of the problem.
From figure 11 we observe that the 'defect' numerics are adept at capturing the well-known traits of Holmboe instability. Linear stability predicts presence of 2 unstable modes of same growth-rate but opposite phase-speed. As expected the numerical solutions do exhibit the beating phenomena between these 2 waves. As visible clearly from figure 11(c)-(d) onwards both the buoyancy and vorticity field has presence of elongated cusp-like structures and one can see both waves before moving past each other. Even at a much later time (figure 11(e)-(f)) the cusps refuse to disappear. If one takes a look at the evolution of disturbance amplitude, $< |\psi|^2 >^{1/2}$, (figure 12) the persistent beating pattern is immediately obvious. One cannot also help but notice in figure 11(e) the inefficient nature of mixing of the buoyancy field by Holmboe waves.
A qualitative comparison of the buoyancy field during Holmboe instability computed using 'defect' numerics with those obtained from experiments and 3D DNS[3][9] can be seen in figure 13. Though the experiments and numerics are not in the exact parameter regime as the 'defect' simulation, it is reaffirming to observe the present calculations ability to

[3]Both experiments and numerics were done for Reynolds number, Re=630, Richardson number being 0.3 and Prandtl number (temperature equivalent to Sc) kept at 700 for experiment and 25 for numerics.

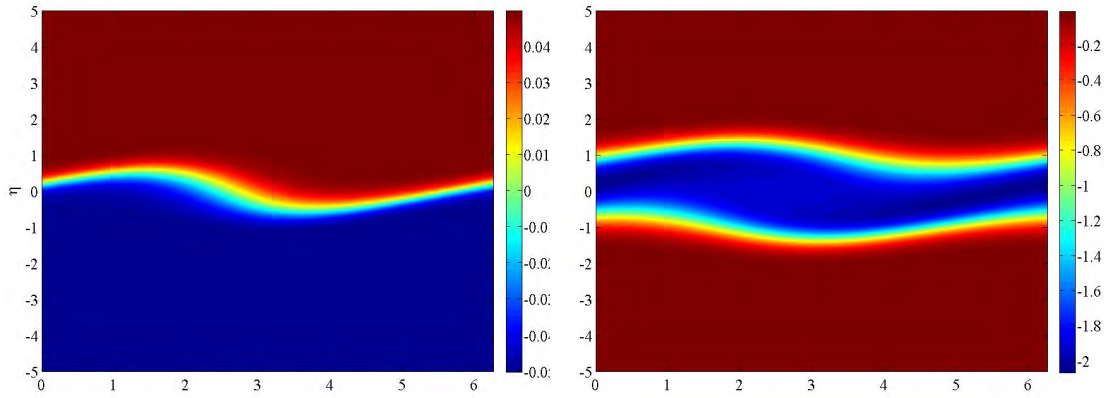

(a) $\mathcal{B}, t = 7$ (b) $\mathcal{Z}, t = 7$

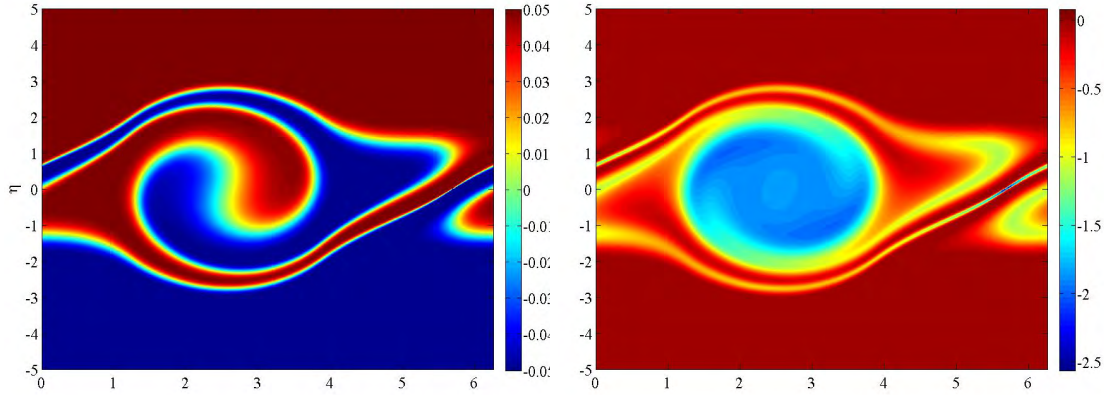

(c) $\mathcal{B}, t = 12$ (d) $\mathcal{Z}, t = 12$

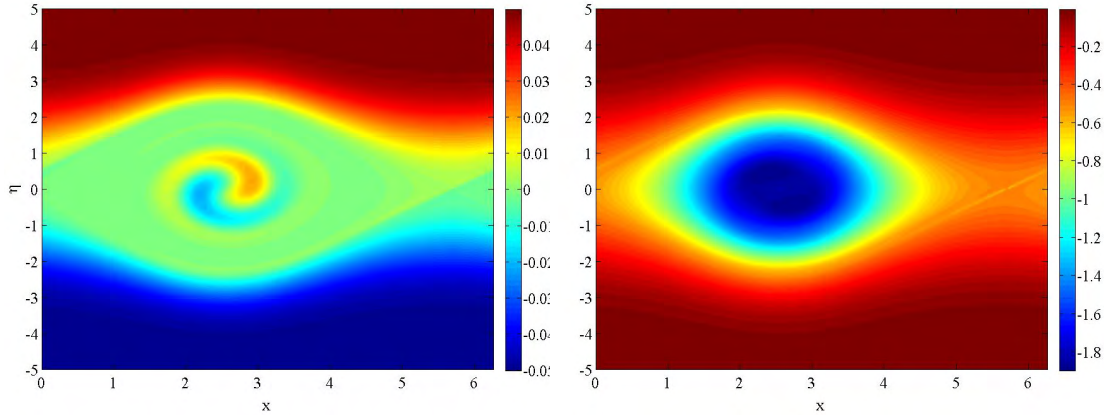

(e) $\mathcal{B}, t = 80$ (f) $\mathcal{Z}, t = 80$

Figure 9: Vorticity and buoyancy fields at different instants of time for stratified KH instability, $f = 2, d = 0.1, k = 1, \Delta = 1/3, \eta_0 = 1$.

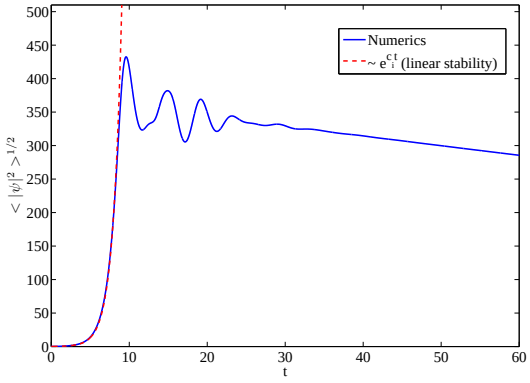

Figure 10: Evolution of disturbance amplitude for stratified KH. $c_i = 0.9035$

reproduce the principal signature of the shear layer with its cuspy arms as visible in others.

5.3.3 Holmboe-KH transition ($d = 1.5$)

Will the persistent counter-propagating cusps be present irrespective of how weak the stratification is as long as linear stability predicts them? Simulations for $d = 1.5$ as seen in figure 14 answers in negative. $d = 1.5$ is away from the critical stratification ($d_{crit} = 0.5$) required for transition from KH to Holmboe as predicted by linear stability. Cusps get formed as expected but as visible in figure 14(a)-(b) the cusps while moving past each other interact nonlinearly and lock each other. Later (figure 14(c)-(d)) these locked waves overturn leading to stirring of the buoyancy field leading towards a KH billow-like stage ((e)-(f)). One can find reference to such nonlinear locking and subsequent overturning/mixing in the experiments of Hogg and Ivey[19]. It is encouraging to see that the reductive model obtained can capture such intricate nonlinear dynamics at very low computational cost.

5.4 Taylor-Caulfield (TC)

Instability due to interaction of gravity waves via shear was one of the intriguing aspects of Taylor's (1931) analysis. It belied conventional belief that one needed an vorticity maxima in the flow or unstable stratification to induce instability in stratified shear flow. Moreover the observations of staircase formation in shear flows provides a strong motivation to understand how do multilayer density profiles interacts with shear. Though Taylor introduced the problem as a canonical stratified shear intability it wasn't until through a series of papers by Caulfield and co-workers (linear stability[10], experiments[11] and DNS[23]) that a great deal was known about the interaction of multilayer density profiles with unbounded shear and mixing layer. The present section will be focused on unbounded shear while mixing layer will be reserved for the next section.
The profile chosen for instability corresponds to the one already dealt before in the linear stability study -

$$N^2 = \frac{d}{2\Delta}\left[\mathrm{sech}^2\left(\frac{\eta - \eta_0}{\Delta}\right) + \mathrm{sech}^2\left(\frac{\eta + \eta_0}{\Delta}\right)\right] \tag{67}$$

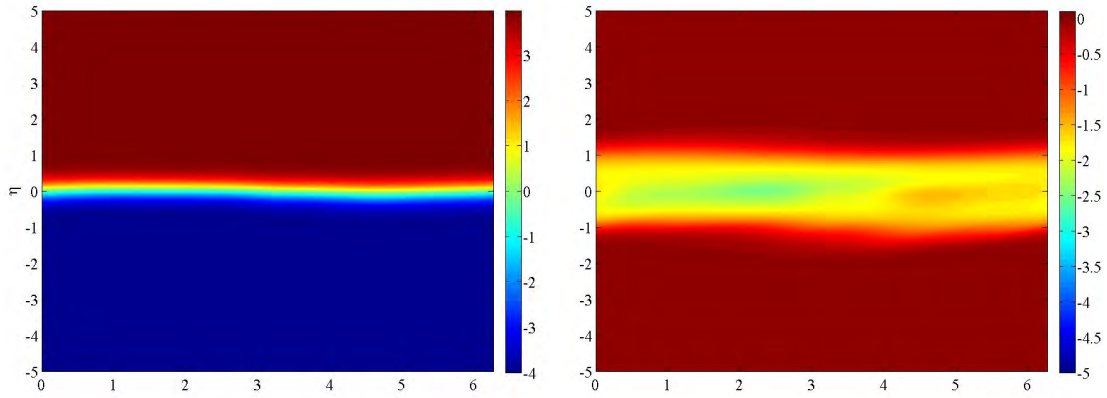

(a) $\mathcal{B}, t = 13$ (b) $\mathcal{Z}, t = 13$

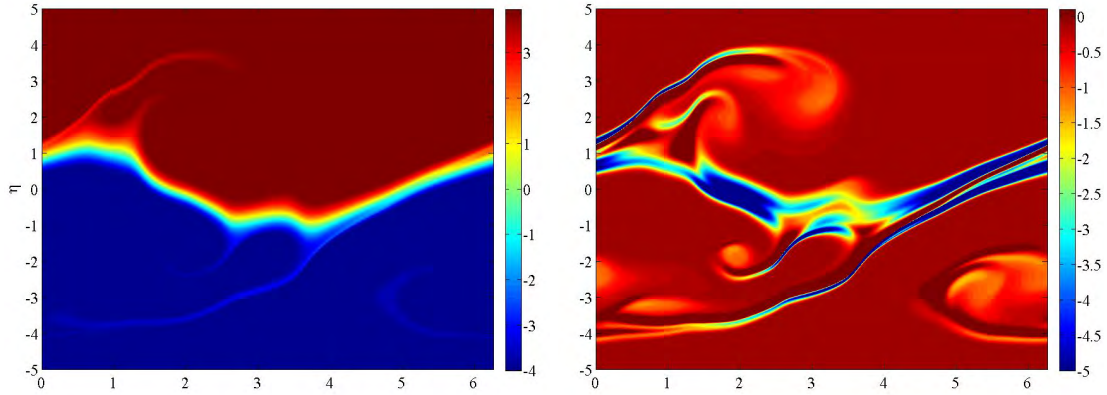

(c) $\mathcal{B}, t = 21$ (d) $\mathcal{Z}, t = 21$

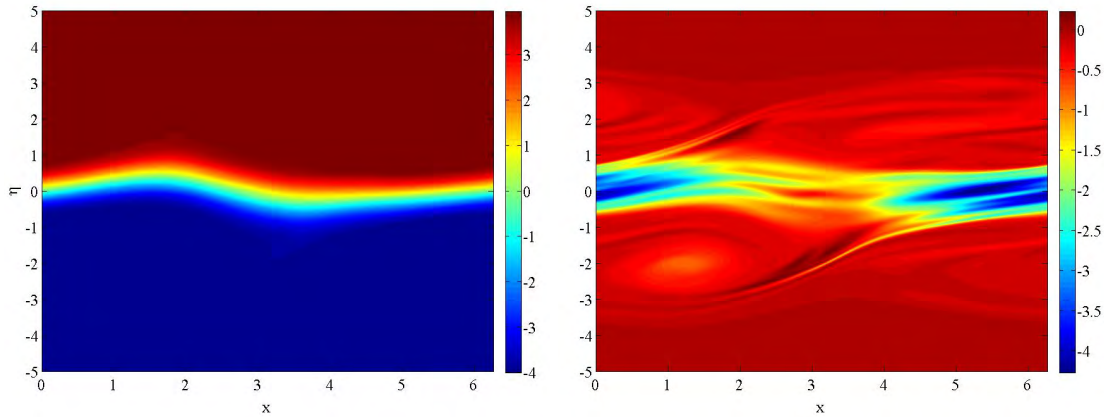

(e) $\mathcal{B}, t = 75.5$ (f) $\mathcal{Z}, t = 75.5$

Figure 11: Vorticity and buoyancy fields at different instants of time for pure Holmboe instability, $f = 2, d = 8, k = 1, \Delta = 1/3, \eta_0 = 1$.

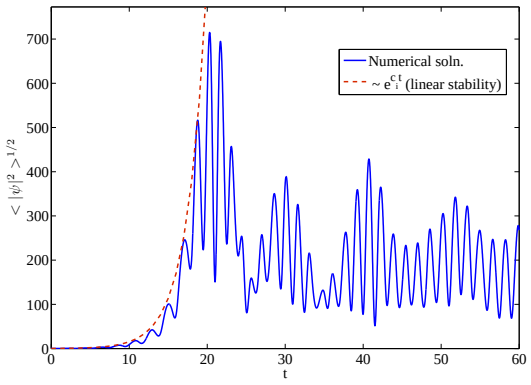

Figure 12: Evolution of disturbance amplitude for pure Holmboe instability. $c_i = 0.4005$

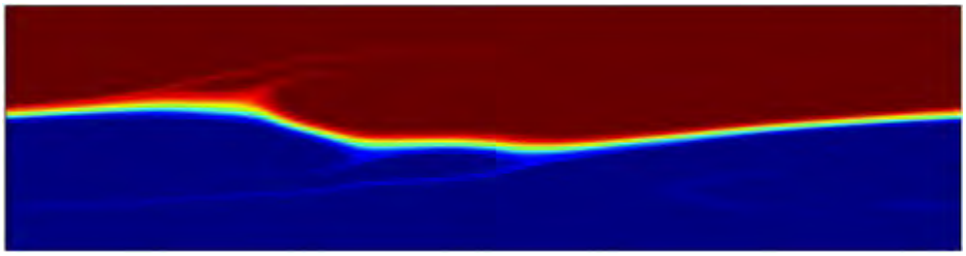

(a) 'Defect' theory

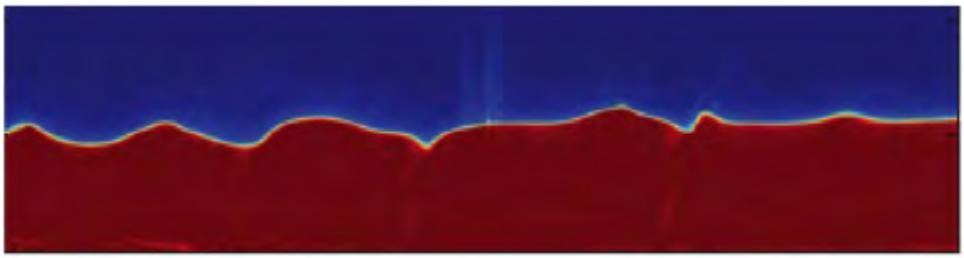

(b) Experimental results

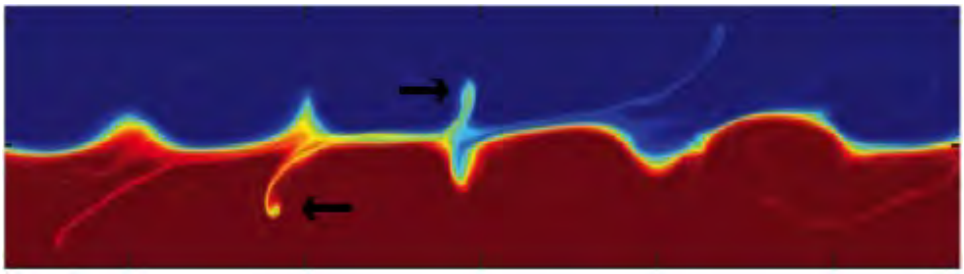

(c) 3D DNS

Figure 13: Qualitative comparison of buoyancy field as obatined from 'defect' theory and that of both experiments and DNS (Carpenter et al.[9])

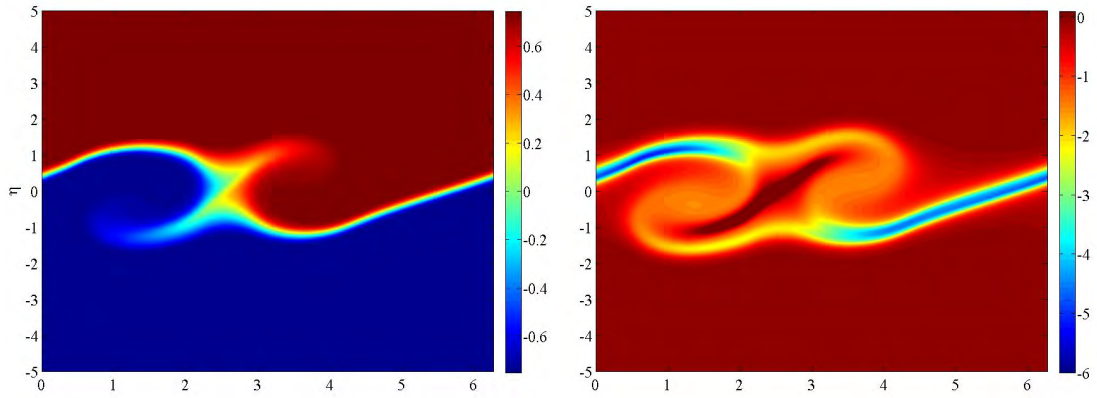

(a) $\mathcal{B}, t = 13.5$ (b) $\mathcal{Z}, t = 13.5$

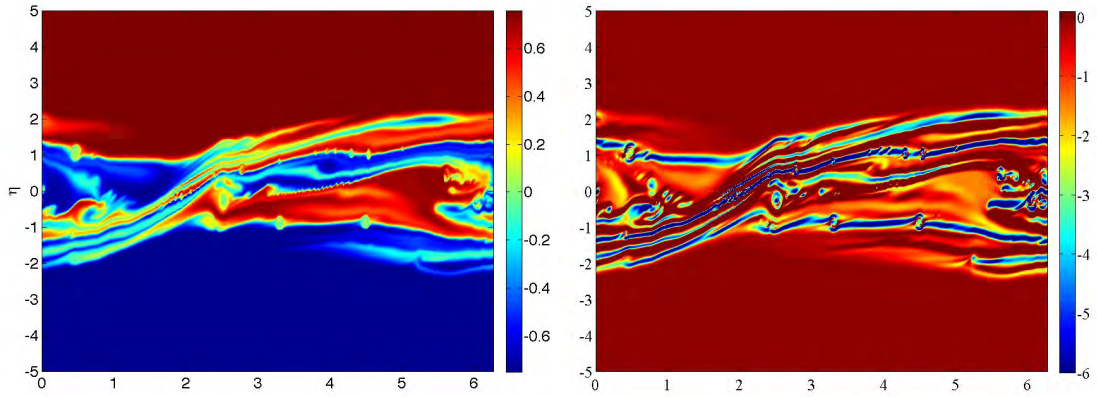

(c) $\mathcal{B}, t = 21$ (d) $\mathcal{Z}, t = 21$

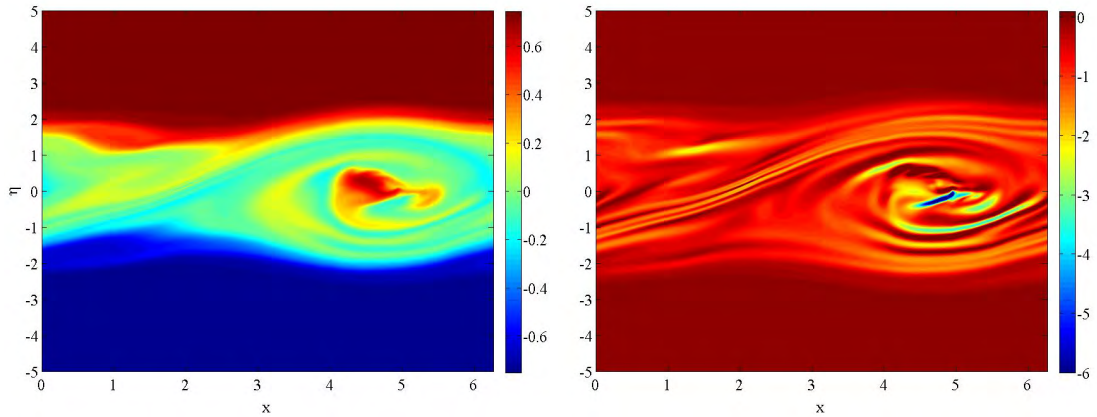

(e) $\mathcal{B}, t = 62.5$ (f) $\mathcal{Z}, t = 62.5$

Figure 14: Vorticity and buoyancy fields at different instants of time for Holmboe-KH transition, $f = 2, d = 1.5, k = 1, \Delta = 1/3, \eta_0 = 1$.

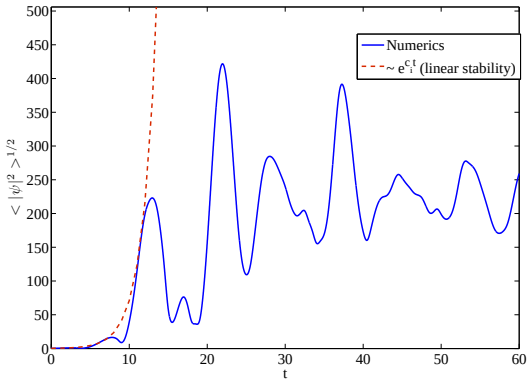

Figure 15: Evolution of disturbance amplitude for Holmboe-KH transition.$c_i = 0.5537$

for the parameters $d = 5, k = 1, \Delta = 1/3, \eta_0 = 2$. The base-state has been seeded with purely buoyancy perturbation and vorticity gets produced purely due to baroclinic effects. During the linear instability stage the baroclinically generated vorticity from the initial conditions gets accumulated at the density interfaces and amplifies (figure 16(a)-(b)). Once the stationary TC waves get nonlinearly saturated the buoyancy forms a billow which too exhibits nutation (figure 16(c), (d) and (f)). The billow formation in TC instability does not involve the extensive overturning as observed in stratified KH but is a more efficient mixing process than pure Holmboe waves (figure 16(e)).

5.5 TC-Holmboe transition

Finally let us consider a 3-layer density profile embedded inside a mixing layer. The extent of the density layer is taken to be smaller than that of the mixing layer (figure 17).

$$F = \frac{f}{2}\left[\tanh\left(\frac{\eta-\eta_2}{\Delta}\right) - \tanh\left(\frac{\eta+\eta_2}{\Delta}\right)\right] \tag{68}$$

$$N^2 = \frac{d}{2\Delta}\left[\mathrm{sech}^2\left(\frac{\eta-\eta_1}{\Delta}\right) + \mathrm{sech}^2\left(\frac{\eta+\eta_1}{\Delta}\right)\right] \tag{69}$$

Simulation has been carried out for $f = 2, d = 4, k = 1, \Delta = 1/3, \eta_1 = 1, \eta_2 = 2$. Linear stability predicts 3 unstable modes - a faster growing stationary TC mode and a pair of slowly growing propagating Holmboe wave. Figure 18(a)-(b) shows the formation of a billow in the initial stages which starts spewing out cusps along its cusps ((c)-(d)). This cuspy billow persists and once again a typical Holmboe feature - beating amplitude pattern (figure 19) - can be seen. Thus if one were to do an experiment on such a profile, a propagating instability would be observed despite linear stability making predictions for a stationary billow. Exploration of such interesting scenarios with great ease was made possible by virtue of working with the 'defect' equations.

6 Nonlinear stationary states

For stratified KH and TC instabilities the time-trace for $< |\psi|^2 >^{1/2}$ seems attain a stationary state but for a viscous decay (figure 10 and 16(f)). A qualitative argument for a

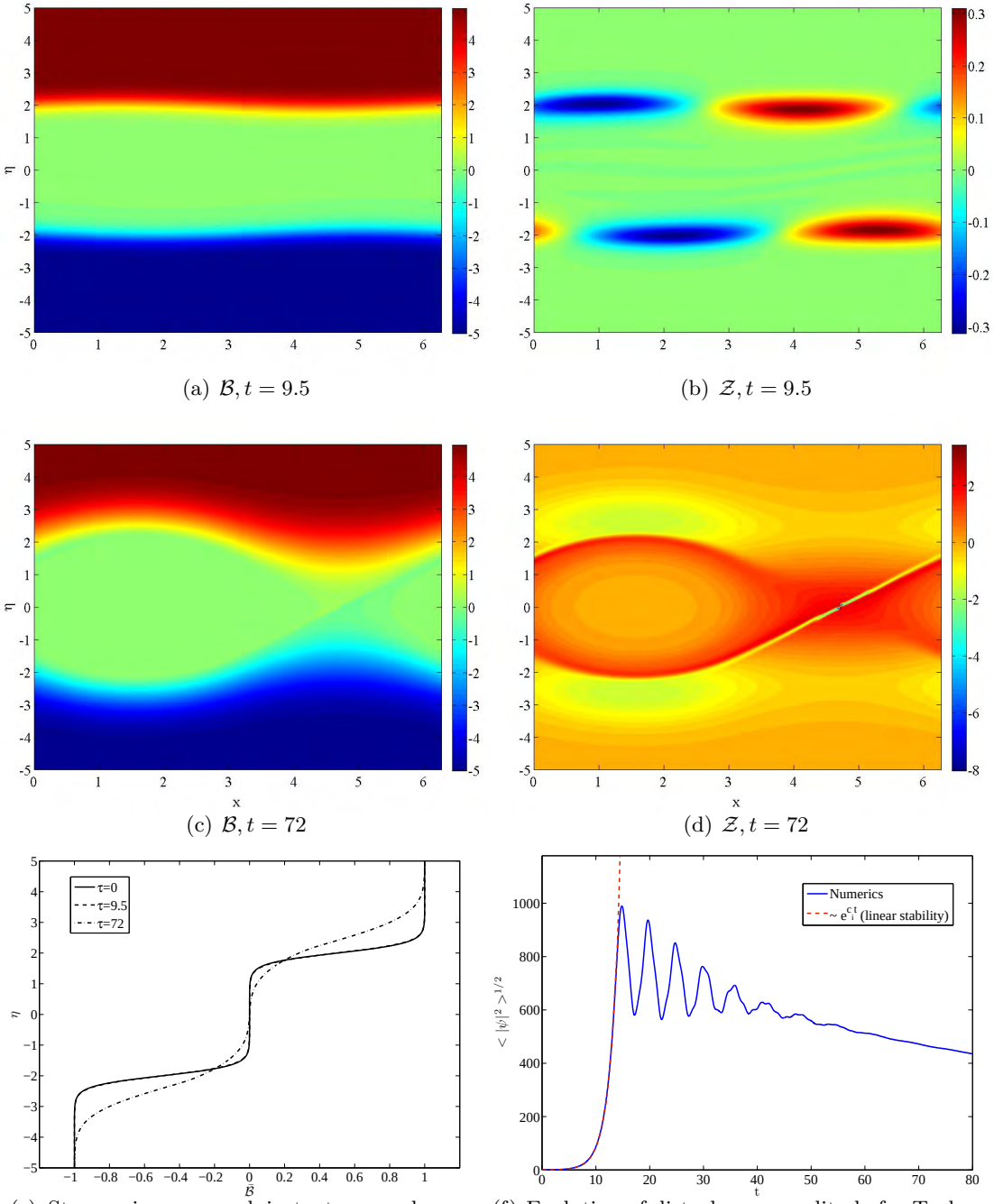

(a) $\mathcal{B}, t = 9.5$

(b) $\mathcal{Z}, t = 9.5$

(c) $\mathcal{B}, t = 72$

(d) $\mathcal{Z}, t = 72$

(e) Streamwise averaged instantaneous buoyancy profile ($\bar{\bullet} = \int \bullet \, dx$) at different instants of time

(f) Evolution of disturbance amplitude for Taylor-Caulfield instability, $c_i = 0.5804$

Figure 16: Vorticity and buoyancy fields at different instants of time for Taylor-Caulfield instability, $d = 5, k = 1, \Delta = 1/3, \eta_0 = 2$.

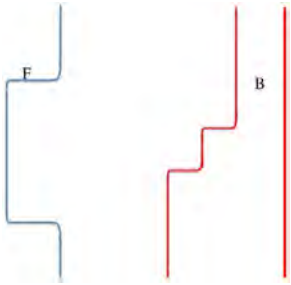

Figure 17: Density layer embedded in a mixing layer (TC-Holmboe transition)

stationary state also receives support when one observes the buoyancy and vorticity plots at the final time computationally attained (figure 9(f) and 16(c)). A time evolution of the plots show that they are remarkably static. Can one provide quantitative confirmations to such guesses?
Let us consider the vorticity-buoyancy defect equation under inviscid, steady[4] assumptions,

$$\eta \mathcal{Z}_x + \Phi_x \mathcal{Z}_\eta = \mathcal{B}_x \tag{70}$$
$$\eta \mathcal{B}_x + \Phi_x \mathcal{B}_\eta = 0 \tag{71}$$

The exact solutions of the above equations are,

$$\mathcal{B} = \mathcal{P}(\mathcal{E}), \tag{72}$$
$$\mathcal{Z} = \mathcal{Q}(\mathcal{E}) + \eta \mathcal{P}'(\mathcal{E}) = \mathcal{Q}(\mathcal{E}) - \mathcal{B}_\eta, \tag{73}$$
$$\text{where,} \qquad \mathcal{E} = -\frac{(\eta - c)^2}{2} + \Phi$$

c being the wave-speed of the state. $\mathcal{P}$ and $\mathcal{Q}$ are arbitrary functionals of the total streamfunction, $\mathcal{E}$. Thus any nonlinear stationary state needs to obey the above functional relationship. We go ahead and try applying this diagnostic on both stratified KH and TC instabilities ($c = 0$ in both cases).
At every instant of time besides $\mathcal{Z}$ and $\mathcal{B}$ the total streamfunction, $\mathcal{E}$, is also computed. Thus at every grid point (x_i, η_k) values of $\mathcal{B}, \mathcal{Z}$ & $\mathcal{E}$ are known. We construct pair of points - $(\mathcal{E}_{ik}, \mathcal{B}_{ik})$ and $(\mathcal{E}_{ik}, (\mathcal{Z} + \mathcal{B}_\eta)_{ik})$. Next all the $(\mathcal{E}, \mathcal{B})[(\mathcal{E}, (\mathcal{Z} + \mathcal{B}_\eta))]$ pairs are plotted in the $\mathcal{B} - \mathcal{E}[(\mathcal{Z} + \mathcal{B}_\eta) - \mathcal{E}]$ planes. If there indeed exists a functional relationship then the scatter of points should collapse on to a curve. That would be a confirmation that the obtained solution is indeed approaching a nonlinear stationary state.
First it is applied on stratified KH (section 5.3.1). As visible from figure 20 the initial functional dependence gets broken and there is a prominent scatter during an intermediate time - an instant of strong instabilities (figure 20(c)-(d)) - before approaching towards a curve (figure 20(e)-(f)). The near horizontal arm(s) in both the buoyancy and vorticity plots corresponds to the uniform region outside the shear layer. From the expression of the

[4]If the state is moving with a constant wave-speed c then a co-moving reference frame is considered. Though not presented here such scenario was observed with simulations for asymmetric stratified shear layer. One of the Holmboe waves is then preferred and the system translates with a constant speed.

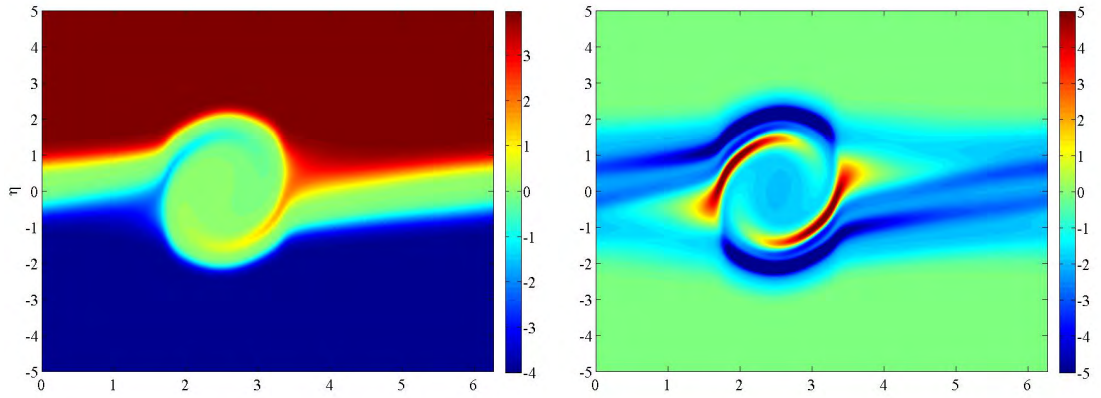

(a) $\mathcal{B}, t = 10.5$ (b) $\mathcal{Z}, t = 10.5$

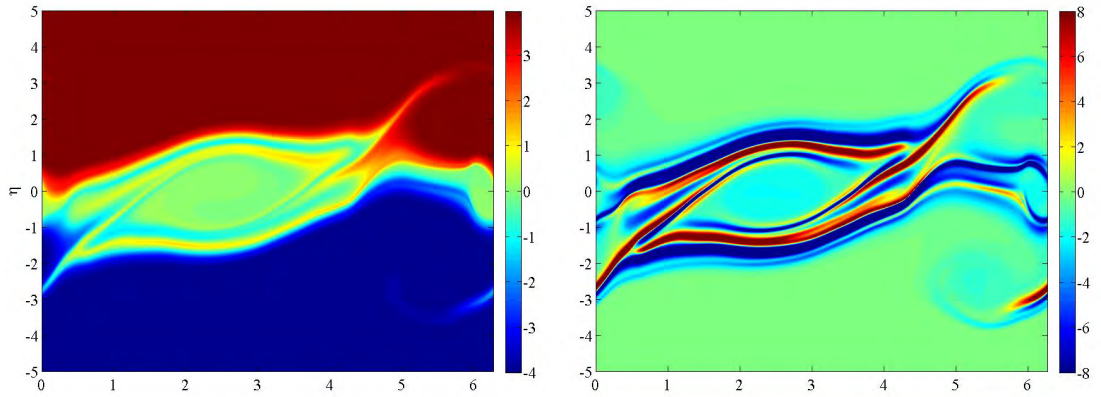

(c) $\mathcal{B}, t = 14.5$ (d) $\mathcal{Z}, t = 14.5$

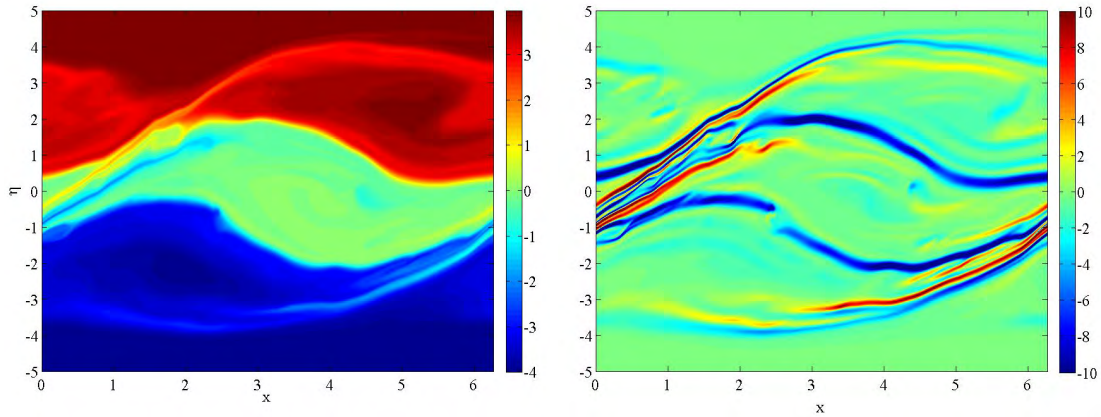

(e) $\mathcal{B}, t = 65.5$ (f) $\mathcal{Z}, t = 65.5$

Figure 18: Vorticity and buoyancy fields at different instants of time for TC-Holmboe transition, $f = 2, d = 4, k = 1, \Delta = 1/3, \eta_1 = 1, \eta_2 = 2$.

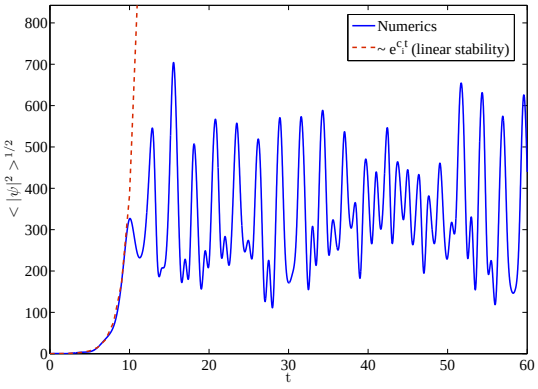

Figure 19: Evolution of disturbance amplitude for TC-Holmboe transition. $c_i = 0.807$

total stream-function, $\mathcal{E}$, one can see why it should be large and negative outside the shear-layer. The vertical region, which hosts most of the dynamics corresponds to the defect. Also the locations from where points seem to spew out vertically, represent the hyperbolic points in the flow. In the last available buoyancy plot, figure 20(e), the bulbous head is representative of the cat's eye region of the flow. As visible from figure 9(e) the $\mathcal{B}$ field has not homogenised completely and there is signature of a dipole-like structure in the cat's eye, which contributes to the bulge.
As seen from figure 21 similar observations are also true for a Taylor-Caulfield case (section 5.4).

Having identified the nonlinear structures the nonlinear stability of the stationary states can be investigated. If we look for stationary points of the energy under the constraints that it has to obey - the conserved quantities determined previously (section 3) - we have the following 'Hamiltonian' (we defer from calling the system Hamiltonian since we have not checked for the Poisson bracket structure for it),

$$\mathcal{H} =< \frac{\eta^2 - \Phi}{2}\mathcal{Z} - \eta\mathcal{B} - c\eta\mathcal{Z} + F(\mathcal{B}) + \frac{c^2}{2}\mathcal{Z} + \mathcal{Z}G(\mathcal{B}) > \tag{74}$$

where $< . >$ denotes average over entire space as defined before. The stationary points of the system are,

$$\frac{\delta\mathcal{H}}{\delta\mathcal{Z}} = 0, \Rightarrow \mathcal{E} = G(\mathcal{B}), \Rightarrow \mathcal{B} = \mathcal{P}(\mathcal{E}) \tag{75}$$

$$\frac{\delta\mathcal{H}}{\delta\mathcal{B}} = 0, \Rightarrow \mathcal{Z} = \frac{\eta - F'(\mathcal{B})}{G'(\mathcal{B})} = \mathcal{Q}(\mathcal{E}) + \eta\mathcal{P}'(\mathcal{E}) \tag{76}$$

confirming what was mentioned in the beginning of this section. Here $\delta\mathcal{H}/\delta\mathcal{Z}$ is the functional derivative of the functional $\mathcal{H}$. To check stability properties we need to check the second variation $\mathcal{H}$.

$$\begin{aligned}\delta^2\mathcal{H} &= < -\delta\psi\delta Z + \{\mathcal{F}''(B) + Z\mathcal{G}''(B)\}(\delta B)^2 + 2\mathcal{G}'(B)\delta Z\delta B > \\ &= < \{\delta Z + \mathcal{G}'(B)\delta B\}^2 + \{-\delta\psi\delta Z - (\delta Z)^2\} + \{\mathcal{F}''(B) + Z\mathcal{G}''(B) - (\mathcal{G}'(B))^2\}(\delta B)^2 >\end{aligned}$$

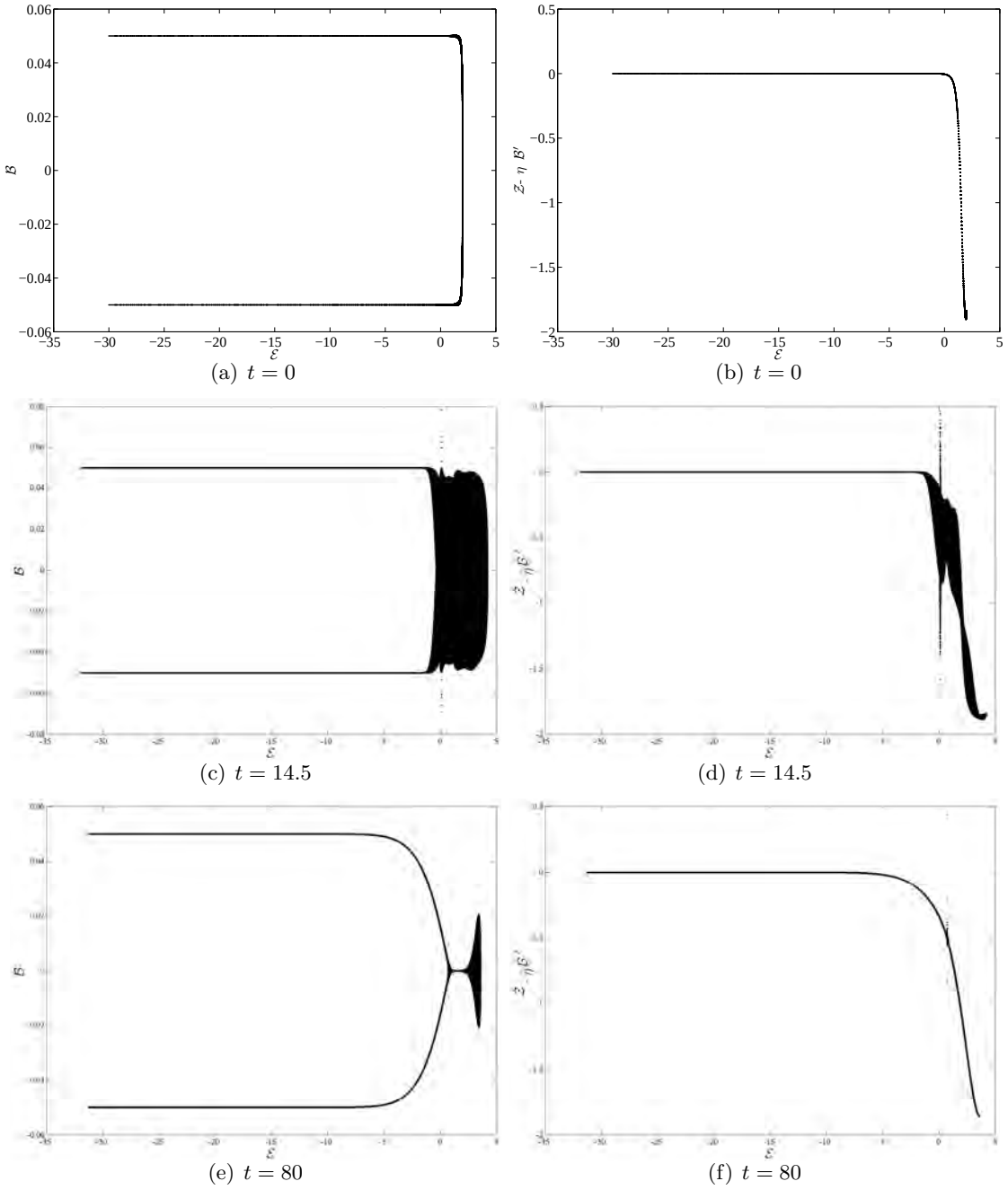

(a) $t = 0$ (b) $t = 0$

(c) $t = 14.5$ (d) $t = 14.5$

(e) $t = 80$ (f) $t = 80$

Figure 20: Nonlinear stationary state diagnostics for stratified KH instability. Time evolution of the dependence of $\mathcal{B}$ with $\mathcal{E}$ is shown in (a), (c) and (e) and that of $\mathcal{Z} - \eta\mathcal{B}'$ with $\mathcal{E}$ in (b), (d) and (f).

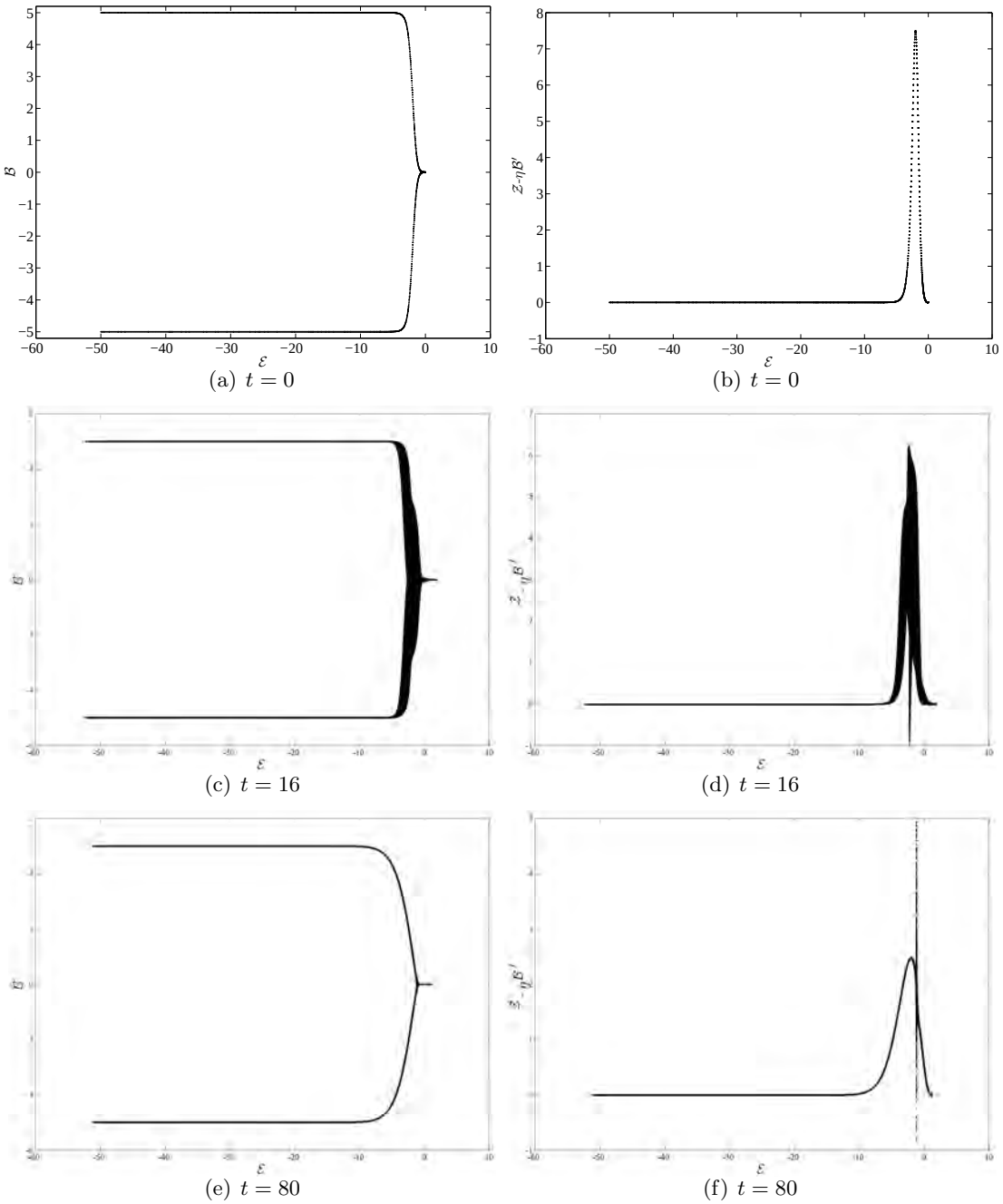

(a) $t = 0$ (b) $t = 0$

(c) $t = 16$ (d) $t = 16$

(e) $t = 80$ (f) $t = 80$

Figure 21: Nonlinear stationary state diagnostics for Taylor-Caulfield instability. Figure description same as figure 20.

In this form a comment cannot be made about nonlinear stability as $\delta^2\mathcal{H}$ is indefinite. But if $\int dxd\eta\{-\delta\psi\delta Z-(\delta Z)^2\}>0$ is positive definite then the condition for stability will be -

$$\{\mathcal{F}''(B)+Z\mathcal{G}''(B)-(\mathcal{G}'(B))^2\}>0$$

Now the question is under what cases is the assumption, $\int dxd\eta\{-\delta\psi\delta Z-(\delta Z)^2\}>0$, true. In 'defect' theory, for an unbounded domain, ψ and Z can be connected in Fourier space as,

$$\hat{\psi}(k,t)=-\frac{1}{2k}\int\hat{Z}(k,\eta,t)d\eta \tag{77}$$

Thus using Parseval's theorem we have

$$\int dx\,d\eta\{-\delta\psi\delta Z-(\delta Z)^2\}>0 \tag{78}$$

$$\Rightarrow\quad \int dk\,d\eta\{-\delta\hat{\psi}\delta\hat{Z}^*-|\delta\hat{Z}|^2\}>0 \tag{79}$$

$$\Rightarrow\quad \int dk\left\{\frac{1}{2k}\left|\int d\eta\,\delta\hat{Z}\right|^2-\int d\eta|\delta\hat{Z}|^2\right\}>0 \tag{80}$$

Presently a detailed study in the above aspects is lacking but it is hypothesized that there would exist a band of wavenumbers in which a stratified shear flow, modelled by 'defect' theory, will be stable. For higher wavenumbers one can always find instability.

7 Conclusion

Exploiting the sharp variations present in stratified shear layers which occurs over small regions, 'defect' vorticity-buoyancy equations have been derived. This equation maintains all the necessary physics - unsteadiness, nonlinearity and viscosity. Linear stability calculations using the 'defect' equations becomes significantly convenient with the present equations. But the big strength of 'defect' equations was found to be in doing nonlinear calculations for various stratified shear layer profiles. Unlike conventional numerics done for Bousinessq Navier-Stokes equations the ones for 'defect' equations can be done with minimum computational effort.

We have been able to explore some interesting cases concerning nonlinear evolution of stratified shear layers. Though a great deal is known about the stratified KH instability, we were able to address some intriguing questions regarding the transition from KH instability to Holmboe waves and also whether a Holmboe instability persists nonlinearly with decreasing stratification. Very little is known about the nonlinear dynamics of Taylor-Caulfield instabilities. An effort has been made to probe TC instability in greater detail while working with 'defect' equations. Coexistence of a TC billow with a Holmboe cusp was also observed while studying density layers embedded in mixing layer.

A diagnostics was used with success to identify nonlinear stationary structures in stratified KH and TC instabilities. Motivated by visual arguments a check was done on the buoyancy, vorticity and total streamfunction field to determine if the flow is attaining an invariant form. Efforts to perform nonlinear stability have so far been inconclusive.

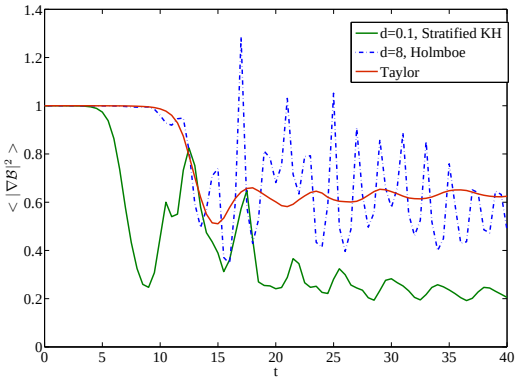

Figure 22: Time evolution of the scalar variance

Being built for flow with sharp interfaces or local distortions, the 'defect' theory has immense potential for stratified shear layer studies. TC instabilities is far from being well-understood and it will be very interesting to explore a wide range of parameter space armed with 'defect' theory. An aspect completely overlooked in the present analysis is the estimation of mixing in the considered flows. Since $Sc \to \infty$ was the domain of interest an estimate of stirring was made based on the scalar variance, $< |\nabla \mathcal{B}|^2 >$. A low value of $< |\nabla \mathcal{B}|^2 >$ denote homegenisation of the scalar field. Figure 22 does indeed highlight an already discussed aspect, based on visual grounds, of mixing/stirring efficiency being maximum for stratified KH, followed by TC and then Holmboe. A more careful analysis needs to be done in this regard and comparisons made with existing DNS and experimental results.
The 'defect' equations are amenable to analytical approaches more easily than the governing equations from which they have been derived. We haven't really used this to obtain the solutions in the nonlinear states in presence of dissipation. A quasi-steady critical layer theory approach is being investigated under the framework of 'defect' equations to answer the asymptotic form of the nonlinear stationary states. Finally a potential future work which has been left out from the present study is the study on the viscous spectrum, issue of quasimodes and transient growth.

8 Acknowledgments

I would like to thank Neil and Colm, without whose patience and constant encouragement this work would not have been possible; Phil Morrison for his help with calculating BGK modes and George for teaching softball lessons to a cricket fanatic. Finally thanks to all the fellows, the staff and the visitors to Walsh Cottage for a wonderful summer.

References

[1] G. K. Batchelor, *Introduction to fluid dynamics*, Cambridge University Press, 1967.

[2] N. J. Balmforth and P. J. Morrison, *Singular eigenfunctions for shearing fluids I*, (1995), Institute for Fusion studies, University of Texas, Austin, Report No. 692.

[3] N. J. Balmforth, D. del-Castillo-Negrete, and W. R. Young, *Dynamics of vorticity defects in shear*. J. Fluid Mech., 333 (1997), pp. 197-230.

[4] N. J. Balmforth, and R. V. Craster, *Dynamics of defects in visco-elastic shear*. J. Non-Newtonian Fluids, 72 (1997), pp. 281-304.

[5] N. J. Balmforth, and W. R. Young, *Long-Wave Instability in Marginally Stable Shear Flows*, Phys. Rev. Lett., 79 (1997), pp. 4155-4158.

[6] N. J. Balmforth, *Stability of vorticity defects in viscous shear*, J. Fluid Mech., 357 (1998), pp. 199-224.

[7] N. J. Balmforth, S. G. Llewellyn Smith and W. R. Young, *Disturbing vortices*, J. Fluid Mech., 426 (2001), pp. 95-133.

[8] J. R. Carpenter, N. J. Balmforth, and G. A. Lawrence, *Identifying unstable modes in stratified shear layers*, Phys. Fluids, 22 (2010), p. 054104.

[9] J. R. Carpenter, E. W. Tedford, M. Rahmani and G. A. Lawrence, *Holmboe wave fields in simulation and experiment*, J. Fluid Mech., 648 (2010), pp. 205-223.

[10] C. P. Caulfield, *Multiple linear instability of layered stratified shear flow*, J. Fluid Mech., 258 (1994), pp. 255-285.

[11] C. P. Caulfield, W. R. Peltier, S. Yoshida and M. Ohtani, *An experimental investigation of the instability of a shear flow with multilayered density stratification*, Phys. Fluids, 7 (1995), p. 3028.

[12] C. P. Caulfield and W. R. Peltier, *The anatomy of the mixing transition in homogenous and stratified free shear layers*, J. Fluid Mech., 413 (2000), pp. 1-47.

[13] C. Z. Cheng and G. Knorr, *The integration of the Vlasov equation in configuration space*, J. Comput. Phys., 22 (1976), pp. 330-351.

[14] S. M. Churilov and I. G. Shukhman, *The nonlinear critical layer resulting from the spatial or temporal evolution of weakly unstable disturbances in shear flows*, J. Fluid Mech., 318 (1996), pp. 189-221.

[15] D. del-Castillo-Negrete, W. R. Young and N. J. Balmforth, *Vorticity dynamics in shear flow*, Proc. 1995 Summer Study Program on Geophysical Fluid Dynamics (ed. R. Salmon). Woods Hole Oceanographic Institution Technical Report.

[16] A. E. Gill, *A mechanism for instability of plane Couette flow and of Poiseuille flow in a pipe*, J. Fluid Mech., 21 (1965), pp. 503-511.

[17] S. Goldstein, *On the stability of superposed streams of fluids of different densities*, Proc. R. Soc. London, Ser. A, 132 (1931), pp. 524-548.

[18] H. Helmholtz, *On discontinuous movements of fluids*, Philos. Mag., 36 (1868), pp. 337-347.

[19] A. McC. Hogg and G. N. Ivey, *The KelvinHelmholtz to Holmboe instability transition in stratified exchange flows*, J. Fluid Mech., 477 (2003), pp. 339-362.

[20] J. Holmboe, *On the behavior of symmetric waves in stratified shear layers*, Geofysiske Publikasjone, 24 (1962), pp. 67-113.

[21] Lord Kelvin, *Hydrokinetic solutions and observations*, Philos. Mag., 42 (1871), pp. 362-377.

[22] G. A. Lawrence, F. K. Browand and L. G. Redekopp, *The stability of a sheared density interface*, Phys. Fluids A, 3 (1991), p. 2360.

[23] V. Lee and C. P. Caufield, *Nonlinear evolution of a layered stratified shear flow*, Dyn. Atmos. Oceans, 34 (2001), pp. 103-124.

[24] J. Lerner and E. Knobloch, *The long-wave instability of a defect in a uniform parallel shear*, J. Fluid Mech., 189 (1988), pp. 117-134.

[25] R. J. LeVeque, *Finite volume methods for hyperbolic problems*, Cambridge University Press, 2002.

[26] O. Pouliquen, J. M. Chomaz and P. Huerre, *Propagating Holmboe waves at the interface between two immiscible fluids*, J. Fluid Mech., 266 (1994), pp. 277-302.

[27] J. W. S. Rayleigh, *On the stability, or instability, of certain fluid motions*, Proc. London Math. Soc., 12 (1880), pp. 57-72.

[28] W. D. Smyth, G. P. Klaassen and W. R. Peltier, *Finite amplitude Holmboe waves*, Geophys. Astrophys. Fluid Dyn., 43 (1988), pp. 181-222.

[29] W. D. Smyth and W. R. Peltier, *Instability and transition in finite-amplitude Kelvin-Helmholtz and Holmboe waves*, J. Fluid Mech., 228 (1991), pp. 387-415.

[30] W. D. Smyth and K. B. Winters , *Turbulence and mixing in Holmboe Waves*, J. Phys. Oceanogr., 33 (2003), pp. 694-711.

[31] K. Stewartson, *The evolution of the critical layer of a Rossby wave*, Geophys. Astrophys. Fluid Dyn., 9 (1978), pp. 185-200.

[32] G. I. Taylor, *Effect of variation in density on the stability of superposed streams of fluid*, Proc. R. Soc. London, Ser. A, 132 (1931), pp. 499-523.

[33] T. Warn and H. Warn, *The evolution of a nonlinear critical level*, Stud. Appl. Maths, 59 (1978), pp. 37-71.